DOKUZ EYLÜL UNIVERSITY
GRADUATE SCHOOL OF NATURAL AND APPLIED SCIENCES

MATHEMATICAL MODELING OF A FLOWING ELECTROLYTE DIRECT METHANOL FUEL CELL BASED ON DIFFERENT FLOW FIELD TYPES

by
Uğur GENÇALP

Ekim, 2017
İZMİR

MATHEMATICAL MODELING OF A FLOWING ELECTROLYTE DIRECT METHANOL FUEL CELL BASED ON DIFFERENT FLOW FIELD TYPES

A Thesis Submitted to the
Graduate School of Natural and Applied Sciences of Dokuz Eylül University
In Partial Fulfillment of the Requirements for the Master of Science of
Department of Mechanical Engineering

by
Uğur GENÇALP

Ekim, 2017
İZMİR

M.Sc THESIS EXAMINATION RESULT FORM

We have read the thesis entitled **"MATHEMATICAL MODELING OF A FLOWING ELECTROLYTE DIRECT METHANOL FUEL CELL BASED ON DIFFERENT FLOW FIELD TYPES"** completed by **UĞUR GENÇALP** under supervision of ASSOC. **PROF. DR. CAN ÖZGÜR ÇOLPAN** and we certify that in our opinion it is fully adequate, in scope and in quality, as a thesis for the degree of Master of Science.

Assoc. Prof. Dr. Can Özgür ÇOLPAN

Supervisor

Prof. Dr. Aytunç Erek

(Jury Member)

Asst.Prof.Dr. Hadi Ganjehsarabi

(Jury Member)

Prof.Dr. Emine İlknur CÖCEN
Director
Graduate School of Natural and Applied Sciences

ACKNOWLEDGMENT

First of all, I am so grateful for my academic supervisor, Assoc. Prof. Dr. Can Özgür ÇOLPAN, who provided me the opportunity to work on this research. His guidance and support have a great share in the creation of this thesis.

Secondly, I would like to thank you my colleague Dr. David OUELLETTE for sharing his knowledge about fuel cell modelling.

I would like to thank my family, especially my wife Duygu, without whose love and support, this work would have been completely impossible.

Also, I would like to thank my precious teachers Prof. Dr. Aytunç Erek and Assoc. Prof. Dr. Hadi Ganjehsarabi for their support in my thesis

Finally, the financial support from TUBITAK (The Scientific and Technological Research Council of Turkey) is greatly acknowledged.

Uğur GENÇALP

MATHEMATICAL MODELING OF A FLOWING ELECTROLYTE DIRECT METHANOL FUEL CELL BASED ON DIFFERENT FLOW FIELD TYPES

ABSTRACT

Direct methanol fuel cells (DMFCs) are seen as the most important technology that can replace batteries in new mobile devices. Nevertheless, the methanol crossover from anode to cathode side is the most important drawback to this technology. This methanol crossover affects fuel cell performance negatively by reducing power density and electrical efficiency. Flowing electrolyte method is used to reduce or eliminate the effect of this shortcoming. In this method, the flowing electrolyte, such as sulfuric acid, washes away any methanol that attempts to crossover through cathode side, thus any undesirable chemical reaction on the cathode side does not occur.

In this thesis, three-dimensional single-phase models for direct methanol fuel cell and flowing electrolyte direct methanol fuel cell were developed with the aim of examining their performances. While modelling, conservation (mass, momentum, species) and electrochemical equations are defined in COMSOL, which is commercial package program, based on finite element method. These equations are coupled and solved by Comsol. The direct methanol fuel cell was modeled individually from the geometry of the fuel cell that is in the Dokuz Eylül University test station and validated with experimental data which are received from this test station. Later on, flowing electrolyte direct methanol fuel cell model was created based on DMFC model and analyzed for four different flow channel designs (serpentine, parallel-serpentine, three-serpentine and grid) used on the cathode side and some important output parameters are investigated (polarization curve, oxygen concentration, pressure, velocity, crossover methanol concentration). Then the effect of some important input parameters (methanol flow rate, flowing electrolyte thickness, flowing electrolyte flow rate and cell temperature) are studies for a serpentine flow channel design which gave the best performance for cathode side.

Keywords: Flowing electrolyte, direct methanol fuel cell, modelling, flow field configuration, Comsol

FARKLI AKIŞ KANALINA DAYALI AKAN ELEKTROLİTLİ DOĞRUDAN METANOL YAKIT PİLİNİN MATEMATİKSEL MODELLENMESİ

ÖZ

Doğrudan metanol yakıt pilleri (DMYP), yeni mobil cihazlarda bataryaların yerini alabilecek en önemli teknolojiler arasındadır. Bununla birlikte, anottan katot tarafına olan istenmeyen metanol geçişi, bu teknolojinin en önemli dezavantajıdır. Bu metanol geçişi, güç yoğunluğunu ve elektrik verimliliğini azaltarak yakıt pili performansını olumsuz olarak etkiler. Akan elektrolit bu kusurun etkisini azaltmak veya ortadan kaldırmak için kullanılır. Bu yöntemde, akan elektrolit, örneğin sülfürik asit, katot tarafına doğru geçmeye çalışan herhangi bir metanolü temizler, bu nedenle katot tarafında istenmeyen herhangi bir kimyasal reaksiyon meydana gelmez.

Bu tez çalışmasında, akan elektrolitli doğrudan metanol yakıt hücresi için üç boyutlu tek fazlı modeller performanslarını incelemek amacıyla geliştirilmiştir. Modelleme yapılırken korunum (kütle, momentum, türler) ve elektrokimyasal denklemler, ticari paket program olan COMSOL ‘da sonlu elemanlar yöntemine dayanılarak tanımlanmıştır. Bu denklemler Comsol ile birleştirilir ve çözülür. Dokuz Eylül Üniversitesinde bulunan doğrudan metanollü yakıt pili geometrisi modellenmiş ve test istasyonundan alınan deneysel veriler ile doğrulanmıştır. Daha sonra akan elektrolitli doğrudan metanollü yakıt hücresi modeli, DMFC modeline dayalı olarak oluşturulmuş ve katot tarafında kullanılan dört farklı akış kanalı tasarımları (serpantin, paralel serpantin, üç serpantin ve ızgara) için analizler yapılmıştır ve bazı önemli çıktı parametrelerinin pil performansına etkisi incelenmiştir. (polarizasyon eğrisi, metanol konsantrasyonu, basınç dağılımı, hız dağılımı, katot tarafına olan metanol geçişi, metanol akısı). Sonra, bazı önemli girdi parametrelerinin (metanol akış hızı, akan elektrolit kalınlığı, akan elektrolit akış hızı ve hücre sıcaklığı) etkisi, katot tarafı için en iyi performansı veren serpantin akış kanalı üzerindeki etkisi incelenmiştir.

Anahtar kelimeler: Akan elektrolit, doğrudan metanollü yakıt pili, modelleme, akış kanalı tasarımı, Comsol

CONTENTS

Page

LIST OF FIGURES

Page

LIST OF TABLES

Page

CHAPTER ONE
INTRODUCTION

1.1 Introduction

As the world energy demand grows day by day, the need for more environmentally friendly and more efficient energy production is increasing. The fact that fossil fuels are responsible for CO_2 emissions and that they will be consumed over time, it pushes the technology to use more environmentally friendly, more energy efficient and sustainable energy resources. Many alternative sustainable energy sources, such as solar, wind, hydroelectric power, bioenergy, geothermal and others have been investigated and developed with their advantages and disadvantages. In addition, many of these energy sources are not portable and cannot be used for transportation. Fuel cells are most promising alternative energy technologies in this years because of being portable, using in transportation, higher energy and electrical efficiency and sustainability.

Fuel cells are one of the most important technologies that will play a role in the production of energy for the future. Fuel cells are electrochemical devices, which are similar to battery, that convert chemical energy into electricity and heat energy. The most important differences from the batteries, they can be fed continuously with fuel and continuous energy production is possible. They have no moving parts, assembling is simple and they work quietly. Some types of fuel cell work at low temperatures (under 100˚C) and thus these fuel cells are suitable for use on electronic devices. And some types of fuel cells, which are operating at high temperatures (500 to 1000˚C), are used in heating as well as generating electrical energy.

1.2 Motivation

Direct methanol fuel cells are considered to be a promising technology for portable applications, and functions by converting the chemical energy stored within

the fuel and oxidant (methanol and oxygen, respectively) to produce electrical energy. The DMFC's performance is limited by several issues, such as slow MOR kinetics and unwanted methanol crossover to the cathode. To solve these issues, several studies have been conducted on the development of different anode catalysts (Zeng & Yang, 2007) and membranes (Baglio, Blasi, Arico, Antonucci & Antonucci, 2004) to improve the MOR kinetics and reduce the methanol permeation, respectively. Another potential solution to the methanol crossover problem is using the flowing electrolyte concept, which was proposed by Kordesch et al. (2001). In this configuration, the flowing electrolyte channel (FEC) and an extra membrane separate the anode and cathode and a dilute electrolyte, such as sulfuric acid, is pumped through FEC to carry away any methanol that attempts to crossover. In addition, an important parameter that influences fuel cell performance in design is the flow channel design. Flow channels help to uniformly distribute the reactants to the catalyst layer, thus helping to maximize the utilization of the catalyst layer. In the literature, many of FE-DMFC performance studies or three-dimensional flow field studies are available. But none of these studies included the effects of the full geometric details of the flow field configuration on a 3D scale. In this thesis, the FE-DMFC with a 25 cm^2 active area is modelled three dimensional, considering all geometric details, and the effect of the cathode flow channel design on the cell performance is investigated.

1.3 Objective

The objective of this thesis is to develop a 3D and single phase FE-DMFC model to study the effects of different cathode flow field configurations on the performance of the fuel cell. As discussed above, there are some FE-DMFC models in the literature; however, none of these studies included the effects of the full geometric details of the flow field configuration on a 3D scale. Firstly, the direct methanol fuel cell was modeled individually from the geometry of the fuel cell that is in the Dokuz Eylül University test station and validated with experimental data which are received from this test station. While modelling, conservation (mass, momentum, species), chemical and electrical equations are defined in COMSOL, which is commercial

package program, based on finite element method. These equations are coupled and solved by Comsol. Later on, flowing electrolyte direct methanol fuel cell model was created based on DMFC model and analyzed for four different flow channel designs (serpentine, parallel-serpentine, three-serpentine and grid) used on the cathode side and some important output parameters are investigated to find the effect of these flow field configurations on the fuel cell performance. Finally, the effects of some important input parameters are studied for a best flow channel design, which gave the best performance for cathode side, to examine the effect of these parameters on cell performance.

1.4 Thesis Outline

In the following section, an overview of fuel cell technology is introduced and detailed information on DMFC is given. FE-DMFC technology is introduced in terms of the operation parameters, performance assessments (polarization curve, loses and components. Finally, Modelling and experimental studies on DMFC and FE-DMFC in the literature are given.

Third chapter includes modelling assumptions, governing equations and boundary conditions which are used in mathematical modelling. Then modelling steps in Comsol is generally discussed.

In the fourth chapter, validation of modelling studies is given and the results of modelling studies for four different flow field configurations are discussed. Effect of some input parameters are studied for the best flow field configuration which is chosen after discussed the results of baseline modelling studies.

The fifth chapter covers the conclusions of the study in this thesis and the suggestions for future studies.

CHAPTER TWO
BACKGROUND AND LITERATURE REVIEW

2.1 Introduction of Fuel Cells

Nowadays, Fuel cells have a wide application and usage area because of efficiency, affordability, silence and environmentally friendly energy production. Fuel cells are electrochemical devices that convert the chemical energy of the fuel being taken up by a fuel converter from alternative sources such as fossil fuels (e.g. coal, oil and natural gas), refinery products, chemical products (e.g. ammonia, methanol, biogas and waste materials) to electricity and heat energy without combustion. The fuel cell systems have about 40-60% of fuel consumption depending on the fuel cell type and the fuel cell efficiency increases up to 80% when the heating temperature is evaluated (Mench, 2008).

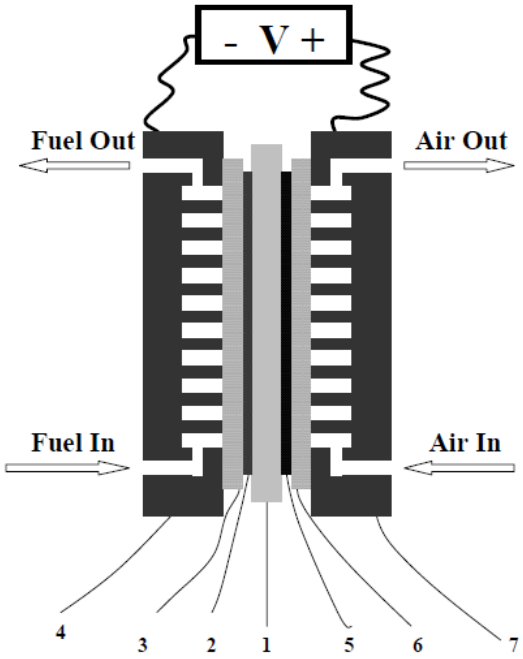

Figure 2.1 Schematic view of the structure of a fuel cell. (1) Electrolyte; (2) anode catalyst; (3) fuel diffusion layer; (4) anode end-plate; (5) cathode catalyst; (6) air diffusion layer; (7) cathode end-plate (Vasquez, 2007)

The fuel cell has the ability to produce electrical energy as long as fuel and oxidizer are provided. Fuel cells can be used in space vehicles, vehicles, marine vehicles, portable devices such as mobile phones, laptop computers, homes, offices, hospitals, hotels and industrial establishments.

2.2 Direct Methanol Fuel Cells

Liquid-fed direct methanol fuel cell (DMFC) is often seen as the most viable alternative to lithium-ion batteries in portable applications because DMFC systems require less auxiliary equipment and can be made simpler than H_2 PEFC. In addition, the storage of methanol is easier compared to other fuels. Both DMFCs and H_2 PEMFCs (Polymer electrolyte membrane fuel cell) are PEMFCs (both of them use the same membrane) but DMFC uses a liquid methanol water solution at the anode side as fuel.

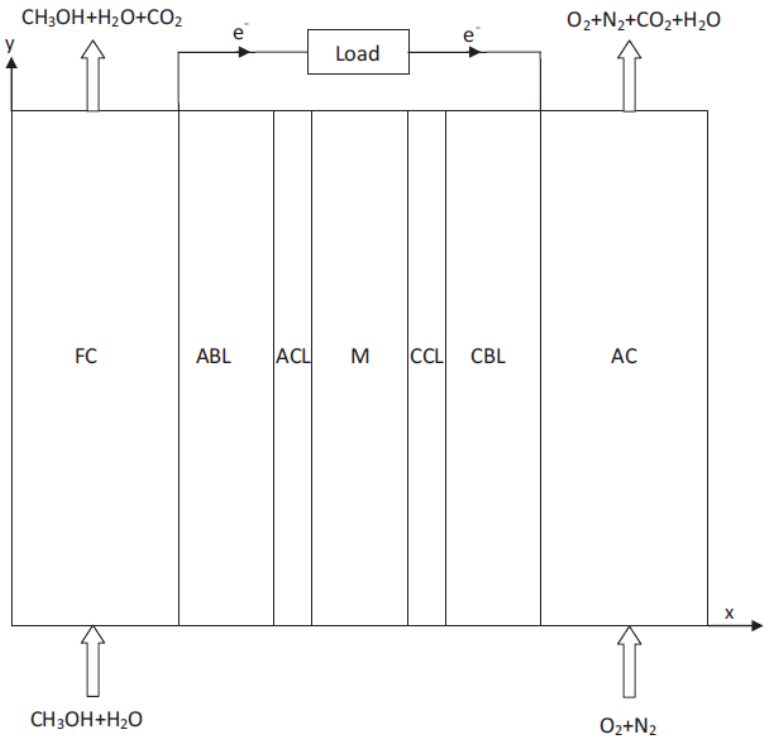

Figure 2.2 Schematic of a 2D cross-section of the DMFC (Colpan, Fung & Hamdullahpur, 2012)

The most negative aspect of the DMFC compared to other fuel cells is that DMFC do achieve high power densities because of the complexities of low temperature methanol oxidation reaction. There are four major technical problems affecting the performance, which are two-phase flow management, methanol crossover, poor catalyst activity and high catalyst loading. One of the most important method used to prevent methanol crossover is flowing electrolyte (Kordesh, 2001).

2.3 Flowing Electrolyte-Direct Methanol Fuel Cells

Although the DMFC is an attractive technology, especially for off-grid portable power applications due to its advantages associated with using liquid methanol solution as the fuel (e.g. easy to store, readily available, and high energy density), the DMFC's performance needs to be further improved for its widespread usage. These performance limitations mainly originate from the problems such as slow MOR kinetics and unwanted methanol crossover from the anode to the cathode. In the latter issue, when methanol crosses over to the cathode, the open circuit voltage (OCV) decreases and the cathodic polarization increases; which in turn reduces the overall performance of the cell. To solve these issues, several studies have been conducted on the development of different anode catalysts and membranes to improve the MOR kinetics and reduce the methanol permeation, respectively.

A potential solution to the methanol crossover problem, discussed above, is using the flowing electrolyte concept, which was proposed by Kordesch et al. (2001). The flowing electrolyte-direct methanol fuel cell (FE-DMFC) is shown schematically in Fig. 1. In this concept, the flowing electrolyte channel (FEC) and an additional membrane separate the anode and cathode sides. A dilute electrolyte, such as sulfuric acid, is pumped through FEC to remove any methanol that attempts to crossover. Therefore, little or no methanol oxidation occurs within the cathode catalyst layer (CCL), the cathodic activation polarization is decreased. However, the Ohmic polarization increases due to the two additional layers (the FEC and the second membrane) in the cell.

2.3.1 Operating Principles of FE-DMFC

Flowing electrolyte-direct methanol fuel cell is schematically shown in Figure 2.3. This figure shows the several layers of the FE-DMFC. The FE-DMFC consists of left to right fuel flow channels (FC), anode backing layer (ABL), anode catalyst layer (ACL), anode membrane (AM), flowing electrolyte channel (FEC), cathode membrane (CM), cathode catalyst layer (CCL), cathode backing layer (CBL) and oxygen flow channel (OC). DMFCs and FE-DMFCs operation principles are almost the same. The only difference is that dilute electrolyte, such as sulfuric acid, is pumped through FEC to carry away any methanol that attempts to crossover.

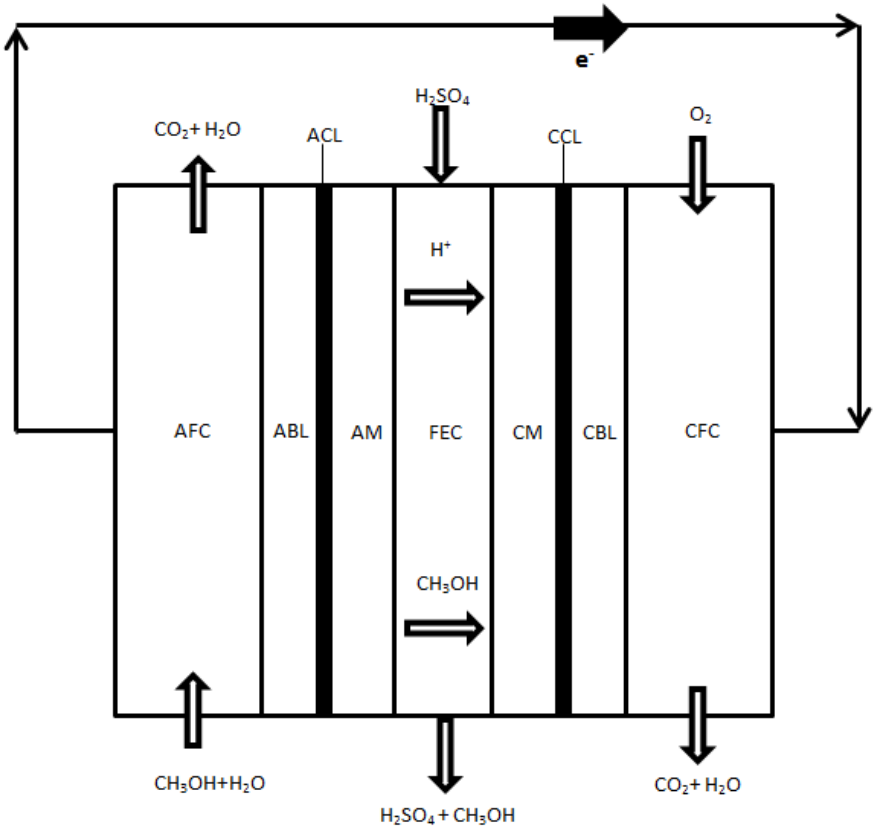

Figure 2.3 Schematic representation of the FE-DMFC

The operation principles of DMFC as follows: diluted methanol solution enters the DMFC from the fuel channel inlet and is diffuses through the ACL (e.g. Pt-Ru / C), ABL (e.g. carbon cloth or carbon paper). In the catalyst layer, the reaction shown

in Eq. (2.1) occurs with the support of catalysts and the methanol solute is separated into protons, electrons and carbon dioxide. Ions move in opposite directions. The protons are transported through the membrane (e.g. Nafion ®) to the CCL, while the electrons transported through the ABL, external load and CBL (e.g., carbon cloth or carbon paper) to reach the CCL, respectively. As can be seen in Eq. (2.2), the transferred ions react with oxygen in the CCL layer. In addition to this reaction, methanol passing through the membrane also enters the reaction with oxygen at CCL as in Eq. (2.3). Thus, the effective area for the reaction shown in Eq. (2.2) is reduced and this unwanted transition leads to an additional voltage loss. Also a portion of the methanol that is passing through the cathode side is dragged by the sulfuric acid and sent out of the battery.

$$CH_3OH + H_2O \rightarrow CO_2 + 6H^+ + 6e^- \quad (2.1)$$

$$1.5O_2 + 6H^+ + 6e^- \rightarrow 3H_2O \quad (2.2)$$

$$\mathrm{CH_3OH} + 1.5\mathrm{O_2} \rightarrow \mathrm{CO_2} + 2\,\mathrm{H_2O} \quad (2.3)$$

2.3.2 Main Components and Materials of FE-DMFC

Flowing electrolyte-direct methanol fuel cell is schematically shown in Figure 2.3. This figure shows the several layers of the FE-DMFC. In the following section, the term and functions of these layers are discussed.

2.3.2.1 Flow Field Plates

Flow channels are located on current collectors which are usually made of graphite. These plates have high electronic and good thermal conductivity and are not affected by the chemical environment inside a fuel cell. Actually, the main tasks of the flow field plate are; current conduction, heat conduction, control of gas flow and product water removal. In the Figure 2.4, there is flow field plate, which has 25 cm^2 active area and made for stack experiments in Dokuz Eylül Üniversitesi.

Figure 2.4 Flow field plate (Personal achieve, 2016)

2.3.2.2 Backing Layers

The backing layers are a porous layer, typically composed of carbon (carbon cloth or carbon paper), which allows the uniform distribution of fuel and oxidant to the catalyst layers. With it, backing layer has some important several of functions (Barbir, 2013);

- Electrically connects the catalyst layer to the bipolar plate and complete the electrical circuit by allowing the passage of electrons
- Provide mechanical support to the MEA

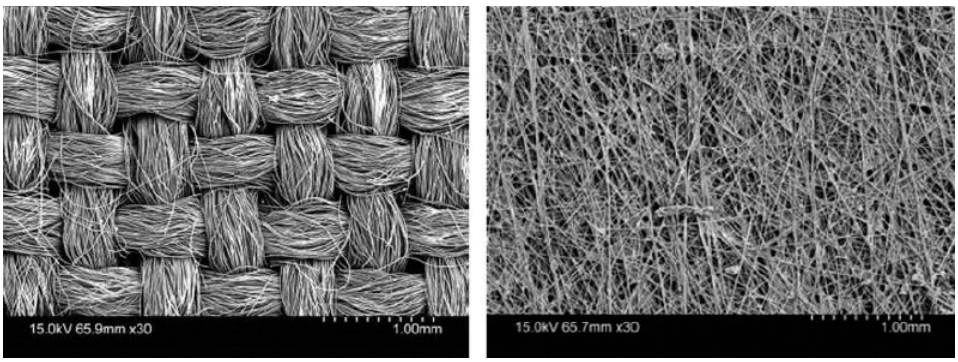

Figure 2.5 SEM micrographs of the carbon cloth (left) and carbon paper (right) (Barbir, 2013)

2.3.2.3 Catalyst Layers

Methanol oxidation reaction (MOR) at the anode side and the oxygen reduction reaction (OOR) at the cathode side occur at the anode and cathode catalyst layers respectively. Platinum-Ruthenium (Pt-Ru) on the anode side and platinum (Pt) on the cathode side are used as catalysts in FE-DMFC. To reduce cell potential loses which is related to the proton transport rate, this layer must be made very thin.

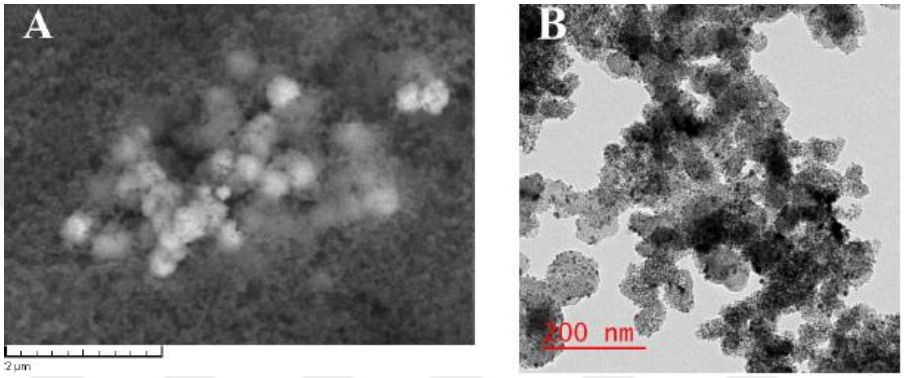

Figure 2.6 In-house micrographs of the cathode catalyst structure. (a) Shows the mesoscale structure observed through SEM, whereas (b) shows the Nano-scale structure which forms the meso-scale structure (Ouellette, 2015)

2.3.2.4 Membrane Layers

A fuel cell membrane must present relatively high proton conductivity, a barrier that prevents mixing of fuel and reactant and must be mechanically and chemically stable. Protonic conductivity is the most important function of polymer membranes used in fuel cells. The best known membrane material for DMFC is Nafion®, produced by Dupont, using perfluoro sulfonyl fluoride ethyl propyl vinyl ether (PSEPVE). Figure 2.7 shows the structure of the Nafion membrane.

2.3.2.5 Flowing Electrolyte Channel

The flowing electrolyte channel (FEC), such as sulfuric acid, separates the anode membrane and cathode membrane to remove any methanol that attempts to

crossover. Therefore no methanol oxidation occurs within the cathode catalyst layer (CCL), the cathodic activation polarization is decreased (Barbir, 2013).

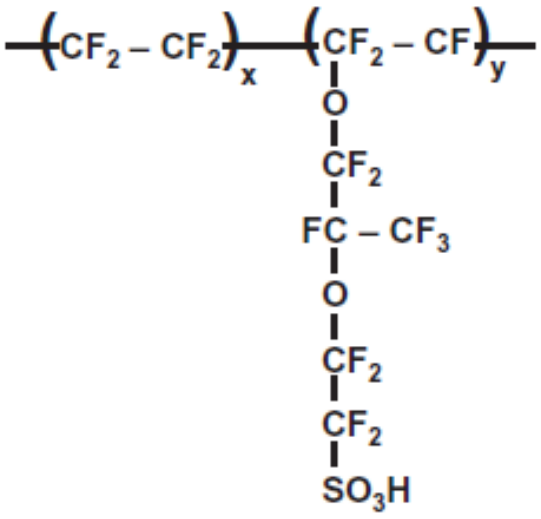

Figure 2.7 Chemical composition of a Nafion membrane (Barbir, 2013)

2.4 Performance Assessment of Fuel Cells

2.4.1 Polarization Curve

The polarization curve, representing the cell voltage-current relationship, is the most important parameter used in evaluating fuel cell performance. As you can see in Figure 2.8, there are five important regions in the polarization curve and each represents different voltage losses (Mench, 2008):

- Activation over-potential losses at the electrodes are represented in zone I.
- Ohmic polarization loses are represented in zone II. These losses include electrical and ionic conductivity losses.
- Concentration polarization loses are represented in zone III. These losses related to the transport limitations of the electrodes.
- The losses in region IV represent the departure from the Nernst thermodynamic equilibrium potential.

- The losses in region V represent the departure from the maximum thermal voltage, a result of entropy change which cannot be engineered.

These voltage losses will be examined in detail in the next section.

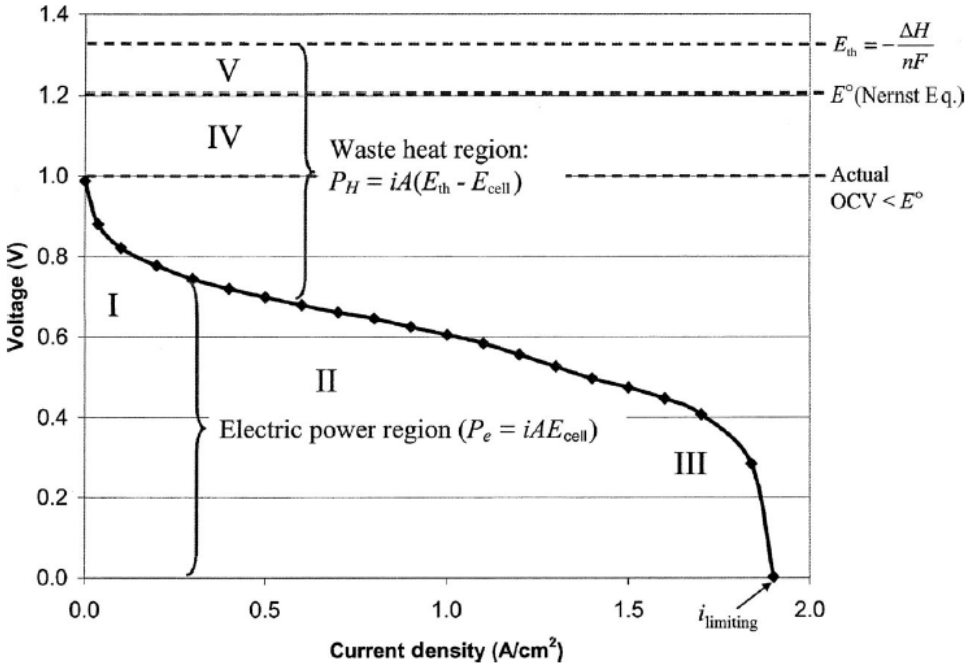

Figure 2.8 Typical polarization curve for fuel cell with significant kinetic, ohmic, concentration and crossover potential losses (Mench, 2008)

2.4.2 Voltage Losses

2.4.2.1 Activation Polarization

The activation polarization, which dominates the loss at low current density, is the voltage required to overcome the activation energy of the electrochemical reaction on the catalytic surface. Physically, activation polarization represents the energy required for the initiation of the reaction. Anodic activation polarization is represented as a $\eta_{a,a}$ and cathodic activation polarization represented as a $\eta_{a,c}$, respectively. The activation polarization losses are effected by the following parameters; reaction mechanism, catalyst type, catalyst layer morphology, operating

parameters, impurities and poisons, species concentrations, age, service history (Mench, 2008).

2.4.2.2 Ohmic Polarization

The ohmic polarization losses are the resistance of each layer to proton and electron conduction. As well as the contact resistance that comes into play due to the contact of the surfaces with each other. Ohmic polarization is represented as a η_{ohmic}. At the beginning of operating life, the ohmic polarization is dominated by ionic conductivity in the electrolyte and catalyst layers. Unless there are aging or assembly / contact problems, the electronic resistance is typically relatively low (Mench, 2008).

2.4.2.3 Concentration Polarization

Concentration polarization occurs with a decrease in the reactant surface concentration, which reduces the thermodynamic voltage from the Nernst equation and the exchange current density from the Butler-Volmer equation. Also concentration this polarization mechanism is related to transport limitation. This limitations are; gas-phase diffusion limitation, liquid-phase accumulation and pore blockage limitation, build-up of inert gases and surface blockage by impurity coverage (Mench, 2008).

2.4.2.4 Other Polarizations

Electrical shorts and species crossover are the other main voltage losses in DMFC. Electrical shorts can occur, if the fuel battery is not well designed or installed properly, which causes voltage loss. On the other voltage loss, physically, a large concentration gradient in the reactant between the anode and cathode sides acts as a driving force for diffusion of reactants across the electrolyte that compete with the opposing electrode reactions, it causes crossover current density (Mench, 2008).

2.5 Literature Survey

2.5.1 Experimental Studies

Sabet-Sharghi et al. (2013) experimentally compared the DMFC with FE-DMFC. They showed that the power density of FE-DMFC decreases when the thickness of flowing electrolyte channel thickness increases. Some researchers have experimentally studied the flow field configuration in a DMFC, such as, Yang et al. (2005); who investigated the effect of anode flow field design on the performance of a DMFC. Their results indicated that the single serpentine flow field delivered better performance than the parallel flow field. Higher cell performance was shown to be achieved at higher methanol flow rates and longer flow channels. However, longer channels caused larger pressure drops across the inlet and outlet. Jung et al. (2009) studied the flow distribution within the cathode flow field; they fabricated and tested grid, parallel and three different types of serpentine designs. The grid flow field configuration showed better gas distribution and minimal pressure drop. Arico et al. (2000) investigated the effects of serpentine and interdigitated flow fields on the DMFC performance. Their experimental results showed that the serpentine flow field gave a lower methanol crossover, higher fuel utilization and slightly larger voltage efficiency at low current densities.

2.5.2 Modelling Studies

Ouellette et al. (2015) developed a single phase and one dimensional FE-DMFC model, which was used to determine the design and operating parameters (inlet concentration of the FE, and flow rate and thickness of FEC) to increase the fuel cell's performance. Higher FE flow rate and FE concentration and lower FEC thickness were found to give the best performance.

Vera (2007) presented 3D/1D model for isothermal single-phase liquid-feed DMFC. 3D model coupled to a 1D model. Polarization curves computed for various

methanol concentration, temperatures and methanol velocities. This model showed good agreement with experimental results.

2.5.3 Flow Field Design Studies

Jung et al. (2007) developed a CFD model of a half-cell DMFC. Their model demonstrated that in parallel flow field design, the performance of the fuel cell was found to decrease quickly at high current densities; and it was found that serpentine type flow field design gave the best performance on the cathode side. Hyun et al. (2006) created a three dimensional, half-cell model to analyse four types of flow fields (parallel, serpentine, parallel serpentine, and zigzag). Their results showed that the zigzag type flow field configuration yielded the most uniform concentration distribution.

2.5.4 Flowing Electrolyte Direct Methanol Fuel Cell Studies

There are several publications in the literature on the development of FE-DMFC through modelling and experimental studies. For example, Kjeang et al. (2005) developed a three dimensional (3D) CFD model that includes the relevant transport phenomena (convection-diffusion mechanisms) in the FEC. They studied the effect of fuel concentration, FEC thickness and flow rate of the sulfuric acid on the methanol crossover rate. Another study by Kjeang et al. (2006), developed a CFD model to analyse the methanol transport within the FEDMFC. Methanol crossover was defined as a flux at the cathode surface in this study. The results of both of these studies showed the benefits of using the flowing electrolyte concept in reducing the methanol crossover problem. Colpan et al. (2011, 2012) developed 1D and 2D models of the FE-DMFC to study the effect of operating parameters (e.g. flowing electrolyte thickness, methanol concentration, and fluid velocity at the fuel, air, and flowing electrolyte channel inlets) on the performance of the fuel cell. The results of these studies showed that when the operating parameters are adjusted to give the highest performance, there is no significant difference between the peak power densities of the DMFC and the FE-DMFC; however, the electrical efficiency of the

cell increases significantly when the FEC outlet is recirculated to the AFC inlet. It was also shown that the FEC thickness has a significant effect on the overall Ohmic polarization of the cell. Therefore, to obtain better performance, this channel must be as thin as possible and the inlet fluid velocity should be as high as possible. Duivesteyn et al. (2013) developed a non-isothermal fuel cell model to observe the effects of the fluid dynamics on the FEC channel and to compare the results with those obtained under isothermal conditions. The results showed that there is no significant temperature difference between the inlet and outlet of the FEC; and it was recommended that a FEC material with lower porosity and higher permeability should be selected to increase the fuel cell performance.

CHAPTER THREE
MATHEMATICAL MODELLING OF FLOWING ELECTROLYTE-DIRECT METHANOL FUEL CELL

3.1 Introduction to Mathematical Modelling

This chapter presents mathematical modelling of three dimensional single phase FE-DMFC. Firstly, computational domain is described. Secondly, Modelling assumptions are given. Then, governing equations and boundary conditions are described in detail. Finally, give information about how to model in Comsol Multiphysics.

3.2 Computational Domain

In Figure 3.1, one of the fuel cell modelled in this study is seen. Single cell FE-DMFC is designed and modelled with all layer. The thicknesses of the layers are modelled by taking the thicknesses of the materials used in the experiments individually (BLs: 210 μm, CLs: 30 μm, AM: 183 μm, CM: 183 μm, and FEC: 610 μm). The fuel and oxygen channels are modeled as a volume.

3.3 Modelling Assumptions

The modelling assumptions in this study are as follows:

- The fuel cell operates under steady state, single phase and isothermal conditions.
- Each media is homogeneous and isotropic.
- All crossed over methanol is fully consumed at the CCL-CM interface.
- The membranes are fully hydrated.
- Gaseous species follow the ideal gas law.
- All flows are assumed to be laminar.
- There are no gas fluxes through the membrane.

- All physical properties are considered constant.
- Gravitational effects are neglected.
- Contact resistances between each layer are ignored.
- The system runs at steady state conditions.

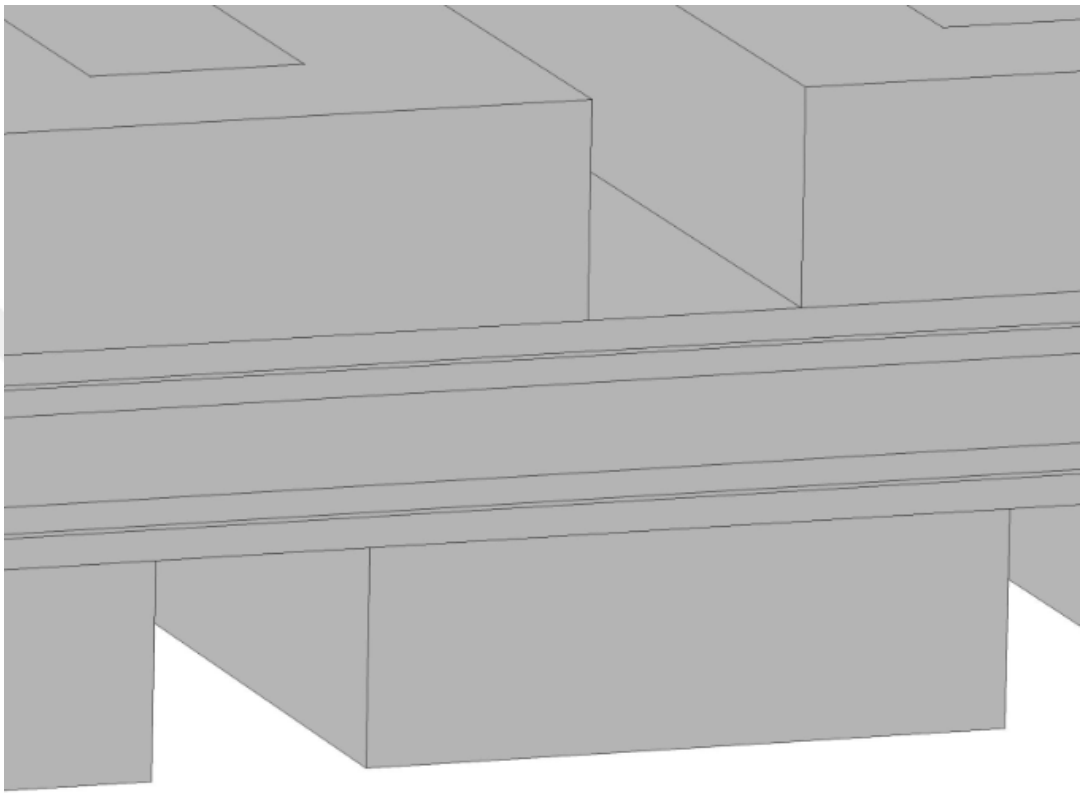

Figure 3.1 Three Dimensional Model for FE-DMFC

3.4 Governing Equations and Boundary Conditions

3.4.1 Conservation of Mass, Momentum and Species

Within the anode and cathode flow fields, the conservation of mass and momentum equations, which are shown in Eq. (3.1) and Eq. (3.2), were employed to calculate the pressure and velocity distributions.

$$\rho(\nabla \cdot \mathbf{u}) = 0 \tag{3.1}$$

$$\rho(\mathbf{u} \cdot \nabla)\mathbf{u} = \nabla\left[-p\mathbf{I} + \mu(\nabla\mathbf{u} + (\nabla\mathbf{u})^{T}) - \frac{2}{3}\mu(\nabla\mathbf{u})\mathbf{I}\right] + \mathbf{F} \tag{3.2}$$

Where ρ is density, p is pressure, μ is dynamic viscosity, u is velocity, I is the identity matrix, and F is the body force vector.

Within the porous layers, the conservation of mass and momentum equations take a slightly different form as given by Eq. (3.3) and Eq. (3.4), respectively. In these equations, the generation and consumption of mass within the catalyst layers as well as the drag caused by the porous structure onto the fluid are accounted for.

$$\rho\nabla\cdot\mathbf{u} = Q_{br} \tag{3.3}$$

$$\frac{\rho}{\varepsilon_p}\left((\mathbf{u}\cdot\nabla)\frac{\mathbf{u}}{\varepsilon_p}\right) = \nabla\cdot\left[-p\mathbf{I} + \frac{\mu}{\varepsilon_p}(\nabla\mathbf{u} + (\nabla\mathbf{u})^T) - \frac{2\mu}{3\varepsilon_p}(\nabla\cdot\mathbf{u})\mathbf{I}\right] - \left(\mu K^{-1} + \beta_F|\mathbf{u}| + \frac{Q_{br}}{\varepsilon_p^2}\right)\mathbf{u} + \mathbf{F} \tag{3.4}$$

Here, ε_p is the porosity, K is the permeability, β_F is the Forchheimer coefficient, and Q_{br} is the mass source.

Eq. (3.5) and Eq. (3.6) are the conservation of chemical species and molar flux of the chemical species of interest, respectively. Here, D is the molecular diffusion coefficient, c is the molar concentration, R_i is the source term which accounts for the creation or consumption of the chemical species, the subscript i refers to an arbitrary species, and N is the molar flux.

$$\nabla.(-D_i\nabla c_i) + \boldsymbol{u}\nabla c_i = R_i \tag{3.5}$$

$$N_i = -D_i\nabla c_i + \boldsymbol{u}c_i \tag{3.6}$$

3.4.2 Electrochemistry

For a given current density, the cell voltage can be calculated using Eq. (3.7), which is the difference between the reversible cell voltage and all of the voltage losses (activation, concentration and Ohmic losses).

$$V_{cell} = V_{rev} - \eta_{act} - \eta_{conc} - \eta_{ohm} \tag{3.7}$$

In this equation, V_{cell} is the cell voltage, V_{rev} is the reversible cell voltage, η_{act} is the summation of the anode and cathode activation polarizations, η_{conc} is the summation of the anode and cathode concentration polarizations, and η_{ohm} is the Ohmic polarization.

On the anode side, the activation polarization is calculated using the Tafel equation, Eq. (3.8).

$$\eta_{act}^{a} = \left(\frac{R.T}{\alpha_a.F}\right) ln\left(\frac{i_{cell}}{i_{oa}}\right) \tag{3.8}$$

Where α_a is the anodic charge transfer coefficient, i_{cell} is the cell current density, and i_{oa} is the anode exchange current density, which can be calculated from Eq. (3.9). In this equation, n is the reaction order, which can be calculated from Eq. (3.10).

$$i_{oa} = i_{oa,ref}\left(\frac{C_l^{MeOH}}{C_{l,ref}^{MeOH}}\right)^n \tag{3.9}$$

$$n = \begin{cases} 0: \ C_l^{MeOH} \geq C_{l,ref}^{MeOH} \\ 1: \ C_l^{MeOH} < C_{l,ref}^{MeOH} \end{cases} \tag{3.10}$$

To estimate the cathodic activation polarization, the Tafel equation is used, following the form shown in Eq. (3.11).

$$\eta_{act}^{c} = \left(\frac{R.T}{\alpha_c.F}\right) ln\left(\frac{i_{cell}+i_{xover}}{i_{oc}}\right) \tag{3.11}$$

Where α_c is the cathodic charge transfer coefficient, i_{oc} is the cathode exchange current density (calculated using Eq. (3.12)), i_{xover} is the crossover current density (calculated using Eq. (3.13)), and $\dot{N}''_{CH_3OH}$ is the molar flux of methanol at the CM-CCL interface (calculated using Eq. (3.14)). The first and second terms in Eq. (3.14) originate from the diffusion and electroosmotic drag mechanisms.

$$i_{oc} = i_{oc,ref}\left(\frac{C_g^{O_2}}{C_{g,ref}^{O_2}}\right) \tag{3.12}$$

$$i_{xover} = 6.F.\dot{N}''_{CH_3OH} \tag{3.13}$$

$$\dot{N}''_{CH_3OH} = -(\varepsilon_{cl}^{1.5}.D_e^{MeOH})(\nabla C_l^{MeOH}) + \varepsilon_{cl}.n_d.\left(\frac{C_l^{MeOH}}{C_l^{H_2O}+C_l^{MeOH}}\right).\frac{i_{cell}}{F} \tag{3.14}$$

To estimate the anodic and cathodic concentration polarizations, the concentration dependency of the Nernst equation is used, following the forms shown in Eqs. (3.15) and (3.16). Here, it is assumed for simplicity that the concentration of the anode and cathode reactants within their respective CLs, and with respect to their inlet values, are the only factors that affect the concentration dependency of the reversible cell voltage.

$$\eta_{conc}^{a} = \left(\frac{R.T}{n_a.F}\right) ln\left(\frac{C_l^{MeOH}}{C_{l,in}^{MeOH}}\right) \tag{3.15}$$

$$\eta_{conc}^{c} = \left(\frac{R.T}{n_c.F}\right) ln\left(\frac{C_l^{O_2}}{C_{l,in}^{O_2}}\right) \tag{3.16}$$

Here, n_a and n_c are the number of electrons transferred in the anodic and cathodic reactions respectively, and the subscript in corresponds to the inlet values of the methanol and oxygen concentrations.

The Ohmic polarization is calculated using Ohm's law as shown in Eq. (3.17).

$$\eta_{ohm} = i_{cell}\left(\frac{t_{ccl}}{\sigma_{ccl}} + \frac{t_{cm}}{\sigma_{cm}} + \frac{t_{fec}}{\sigma_{fec}} + \frac{t_{am}}{\sigma_{am}} + \frac{t_{acl}}{\sigma_{acl}}\right) \tag{3.17}$$

Where t and σ are the layer thickness and ionic conductivity, respectively.

3.4.2 Boundary conditions

At the anode inlet, the anode inlet flow rate and methanol concentration are set, as given by Eqs. (3.18) and (3.19). Then these inputs will be operated parametrically.

$$\dot{Q_A} = 10\ [mL.min^{-1}] \tag{3.18}$$

$$C_{l,in}^{MeOH} = 1000\ [mol.m^{-3}] \tag{3.19}$$

At the anode outlet, the gauge pressure is set to zero and methanol's species conservation equation is specified to have an outlet condition, as given by Eqs. (3.20) and (3.21), respectively. The same types of inlet and outlet boundary conditions are applied to the cathode.

$$P = 0 \tag{3.20}$$

$$n.[-D_l^{MeOH}(\nabla C_l^{MeOH})] = 0 \tag{3.21}$$

Within the FEC, a known inlet flow rate is set, and the methanol concentration is set to zero, as shown in Eqs. (3.22) and (3.23). The FEC outlet uses the same type of outlet boundary conditions as previously described in Eqs. (3.20) and (3.21).

$$\dot{Q_{FEC}} = 10\ [mL.min^{-1}] \tag{3.22}$$

$$C_{in,fec}^{MeOH} = 0\ [mol.m^{-3}] \tag{3.23}$$

All walls are treated with no flux and no slip conditions, as shown in Eqs. (3.24) and (3.25).

$$-n.\dot{N}_i'' = 0 \tag{3.24}$$

$$u = 0 \tag{3.25}$$

Finally, it is assumed that all crossed over methanol is consumed at the CCL-CBL interface, yielding a set methanol concentration of zero, as given by Eq. (3.26).

$$C_{(CCLICBL)}^{MeOH} = 0 \tag{3.26}$$

A summary of reaction based source and sink terms for catalyst layers are shown in Table 3.1. Also the electrochemical and porous properties, and operation parameters used in this study are shown in Table 3.2.

Table 3.1 Summary of reaction-based source and sink terms

Source/ Sink Terms	**Expression**	
	ACL	**CCL**
S_{gen}^{MeOH}	$-\frac{j_{cell}}{6F}$	$-\frac{j_{xover}}{6F}$
$S_{gen}^{O_2}$	0	$-\frac{j_{cell}+j_{xover}}{4F}$
$S_{gen}^{H_2O}$	$-\frac{j_{cell}}{6F}$	$\frac{j_{cell}}{2F}+\frac{j_{xover}}{3F}$
$S_{gen}^{CO_2}$	$\frac{j_{cell}}{6F}$	$-\frac{j_{xover}}{6F}$

Table 3.2 Initial conditions, chemical properties and operation parameters

Parameter	**Value**
Molar concentration of gaseous oxygen at the inlet feed stream	$C_{O2}^{in} = 7.2467\ [mol/m^3]$
Molar concentration of the methanol at the inlet feed stream	$C_{MEOH}^{in} = 1000\ [mol/m^3]$
Cell temperature	$T = 353\ [K]$
Porosity of the FEC	$\varepsilon_{BL} = 0.47$
Porosity of the BLs	$\varepsilon_{BL} = 0.6$
Porosity of the CLs	$\varepsilon_{CL} = 0.4$
Porosity of membranes	$\varepsilon_{M} = 0.28$
Permeability of ABL	$K_{ABL} = 10^{-11}[m^2]$
Permeability of ACL	$K_{ACL} = 10^{-11}[m^2]$
Permeability of CBL	$K_{CBL} = 10^{-11}[m^2]$

Permeability of CCL	$K_{CCL} = 10^{-11}[m^2]$
Permeability of ACL	$K_M = 10^{-18}[m^2]$
Permeability of FEC	$K_{FEC} = 2x10^{-12}[m^2]$
Dynamic viscosity of liquid water	$\mu_{H_2O} = 3.6x10^{-4}\ [kg/(m.s)]$
Faraday's constant	$F = 96485\ [C/mol]$
Electro-osmotic drag coefficient of water	$n_d^{H_2O} = 2.5$
Anodic charge transfer coefficient	$\alpha_a = 0.5$
Anodic charge transfer coefficient	$\alpha_a = 1$
Universal gas constant	$R_u = 8.314[J/mol/K]$
Reference concentration of methanol	$C_{O_2}^{ref} = 0.472[mol/m^3]$
Anode reference exchange current density	$i_{oa,ref} = 30[A/m^2]$
Cathode reference exchange current density	$i_{oc,ref} = 0.006\ [A/m^2]$
FEC inlet flow rate	$\dot{Q}_{FEC} = 10\ [mL/min]$
Anode inlet flow rate	$\dot{Q}_A = 10\ [mL/min]$
Cathode inlet flow rate	$\dot{Q}_C = 150\ [mL/min]$

3.5 Modelling in Comsol

3.5.1 Geometry

The geometry of the fuel cell was built using the SolidWorks program for four different flow channel designs. It is formed in the same way with the other layers and they were assembled together in the Solidworks. It was then transferred to the Comsol program using LiveLink for SolidWorks. Figure 3.2 shows the use of the LiveLink for Solidworks module and Figure 3.3 shows four different flow channel geometries.

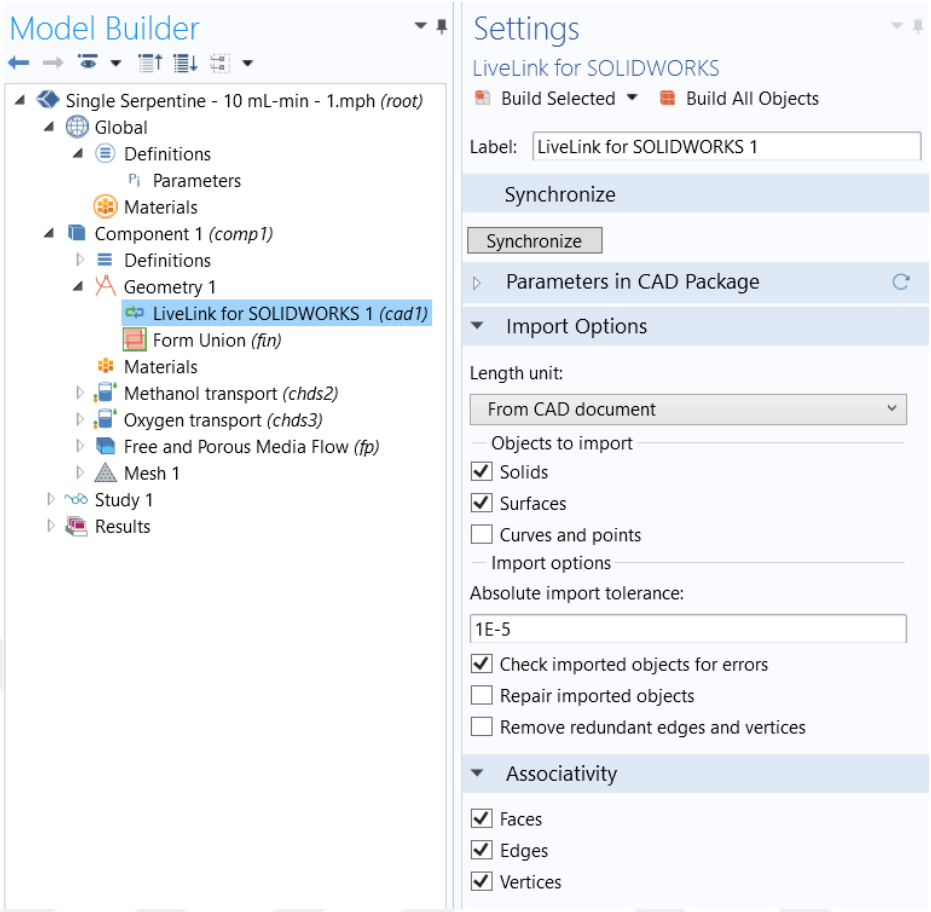

Figure 3.2 LiveLink for Solidworks Using in Comsol

3.5.2 Modelling Procedure

The basic modelling parameters are defined globally in the parameters module. This definition is shown in Figure 3.4. Some equations are not defined in the program and these equations are defined in the program by processing them in the variable module. Some definitions are shown in Figure 3.5. It is also possible to select the volume of these equations to be defined in that volume.

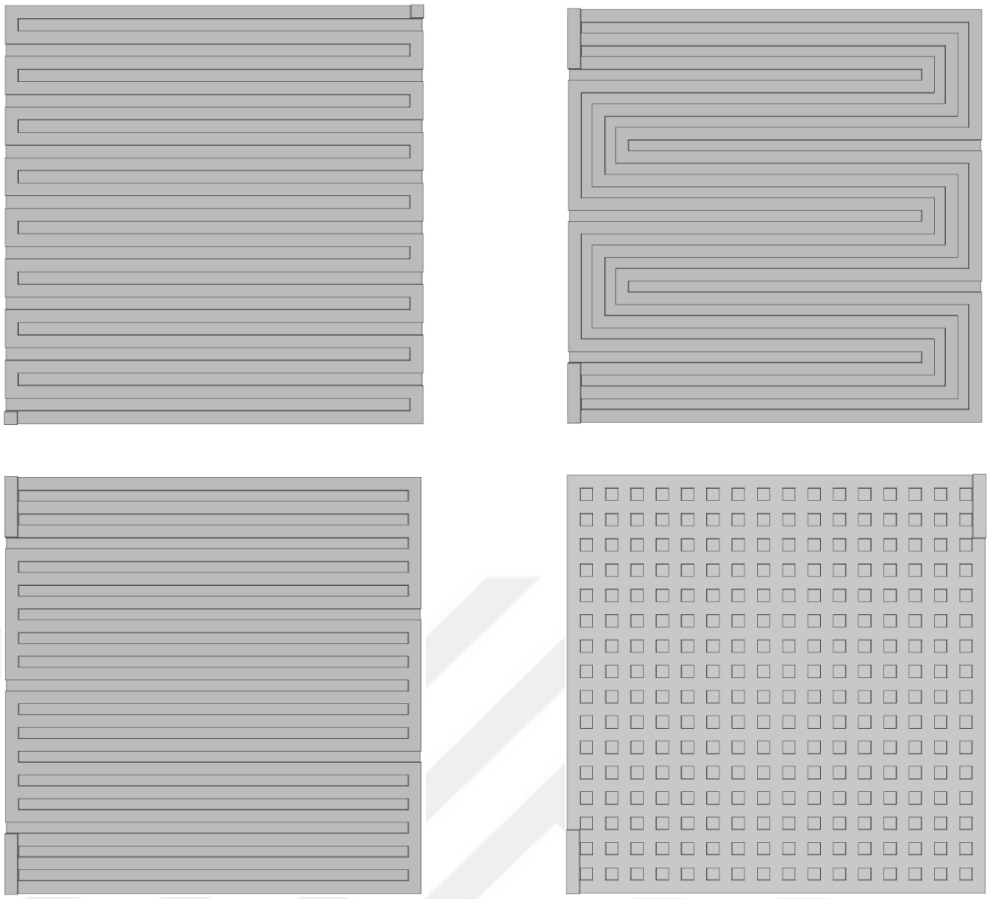

Figure 3.3 FE-DMFC Flow Field Geometries (Serpentine, Three Serpentine, Parallel Serpentine and Grid)

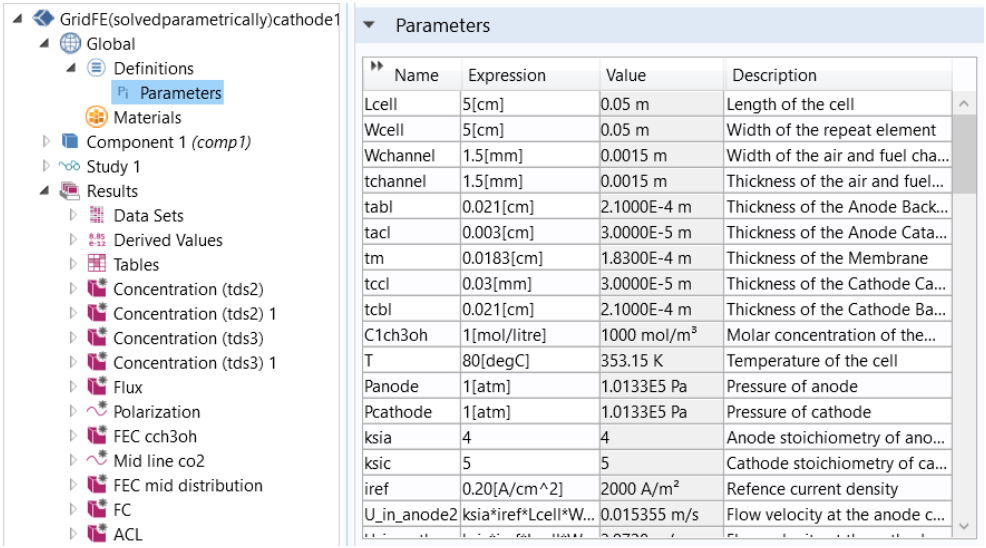

Parameters

Name	Expression	Value	Description
Lcell	5[cm]	0.05 m	Length of the cell
Wcell	5[cm]	0.05 m	Width of the repeat element
Wchannel	1.5[mm]	0.0015 m	Width of the air and fuel cha...
tchannel	1.5[mm]	0.0015 m	Thickness of the air and fuel...
tabl	0.021[cm]	2.1000E-4 m	Thickness of the Anode Back...
tacl	0.003[cm]	3.0000E-5 m	Thickness of the Anode Cata...
tm	0.0183[cm]	1.8300E-4 m	Thickness of the Membrane
tccl	0.03[mm]	3.0000E-5 m	Thickness of the Cathode Ca...
tcbl	0.021[cm]	2.1000E-4 m	Thickness of the Cathode Ba...
C1ch3oh	1[mol/litre]	1000 mol/m³	Molar concentration of the...
T	80[degC]	353.15 K	Temperature of the cell
Panode	1[atm]	1.0133E5 Pa	Pressure of anode
Pcathode	1[atm]	1.0133E5 Pa	Pressure of cathode
ksia	4	4	Anode stoichiometry of ano...
ksic	5	5	Cathode stoichiometry of ca...
iref	0.20[A/cm^2]	2000 A/m²	Refence current density
U_in_anode2	ksia*iref*Lcell*W...	0.015355 m/s	Flow velocity at the anode c...

Figure 3.4 Defining of the basic modelling parameters in COMSOL

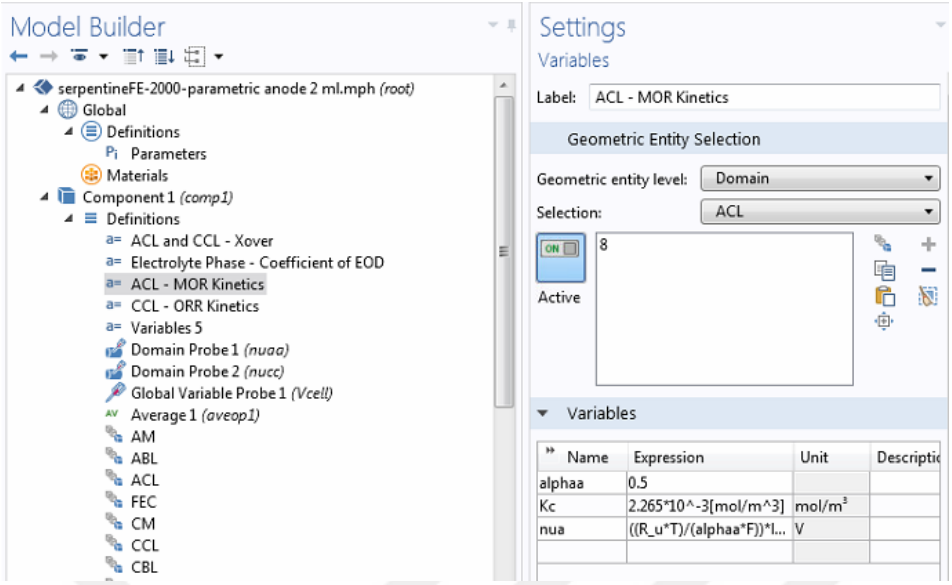

Figure 3.5 Defining of the modelling equations in COMSOL

Continuity and momentum equations are formed by defining the necessary modelling parameters and equations for the steps under the Free and Porous Media Flow module which is shown in Figure 3.6.

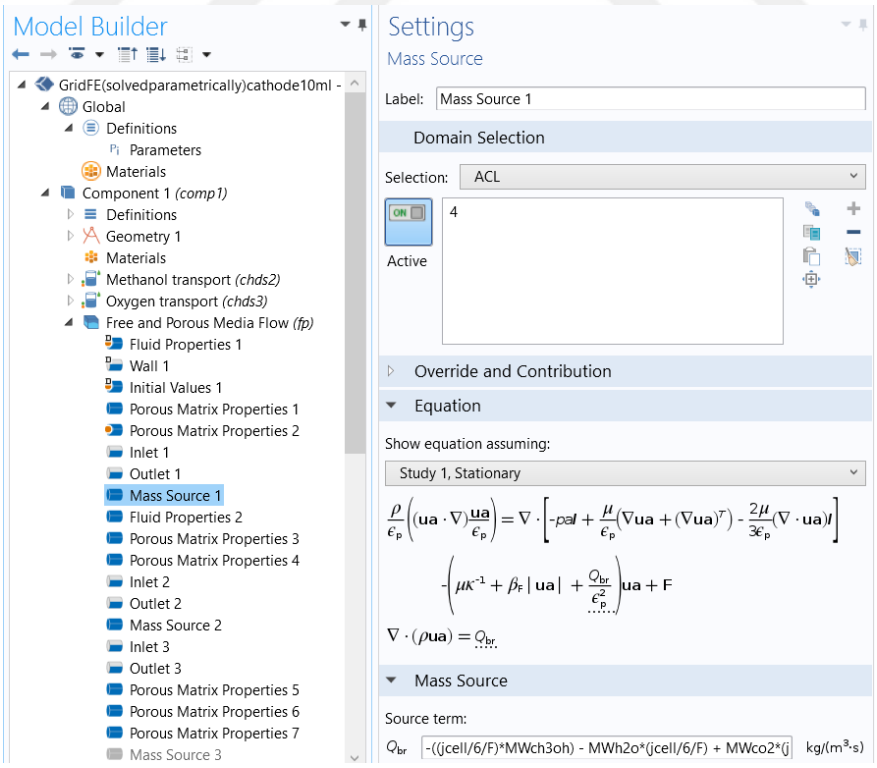

Figure 3.6 Free and Porous Media Flow Modelling Tree in COMSOL

The conservation equations of the species are formed by defining the necessary modelling parameters and equations for the steps under the Transport of Diluted Species module which is illustrated by Figure 3.7

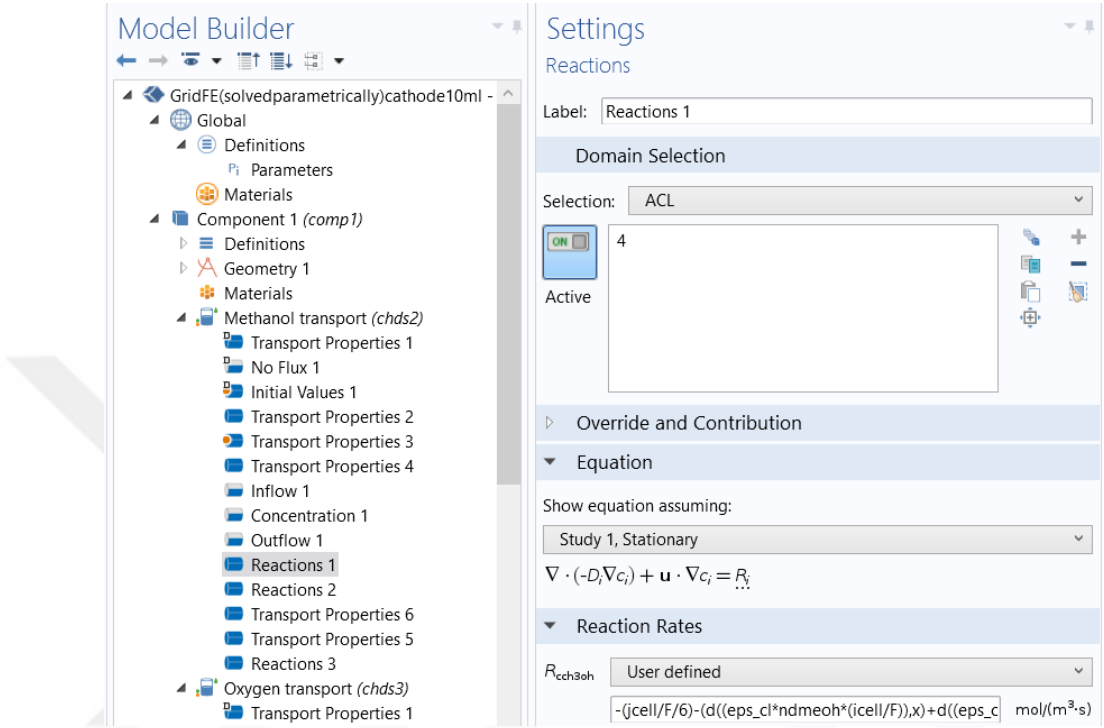

Figure 3.7 Transport of Diluted Species Modelling Tree in COMSOL

3.5.3 Mesh Generation and Solution Procedure

In this study, COMSOL Multiphysics 5.0, a commercially available finite element solver, is used to solve the equations shown above. After entering all the necessary equations using the software's built-in modules (free and porous media flow, and transport of diluted species) and manually entering some equations (e.g. electrochemical relations), the mesh was generated for the geometry. Tetrahedral elements were used to mesh the flow fields and the FEC; whereas triangular elements were used to mesh the remaining layers. Mesh generation in this study is shown in Figure 3.8. Three different segregated groups (concentrations, velocities and pressures) were set up to solve each set of equations using the multifrontal massively parallel sparse (MUMPS) direct solver. It should be noted that the current density of

the cell is take as an input parameter and cell voltage is found after calculating the polarization losses which are a function of the current density of the cell.

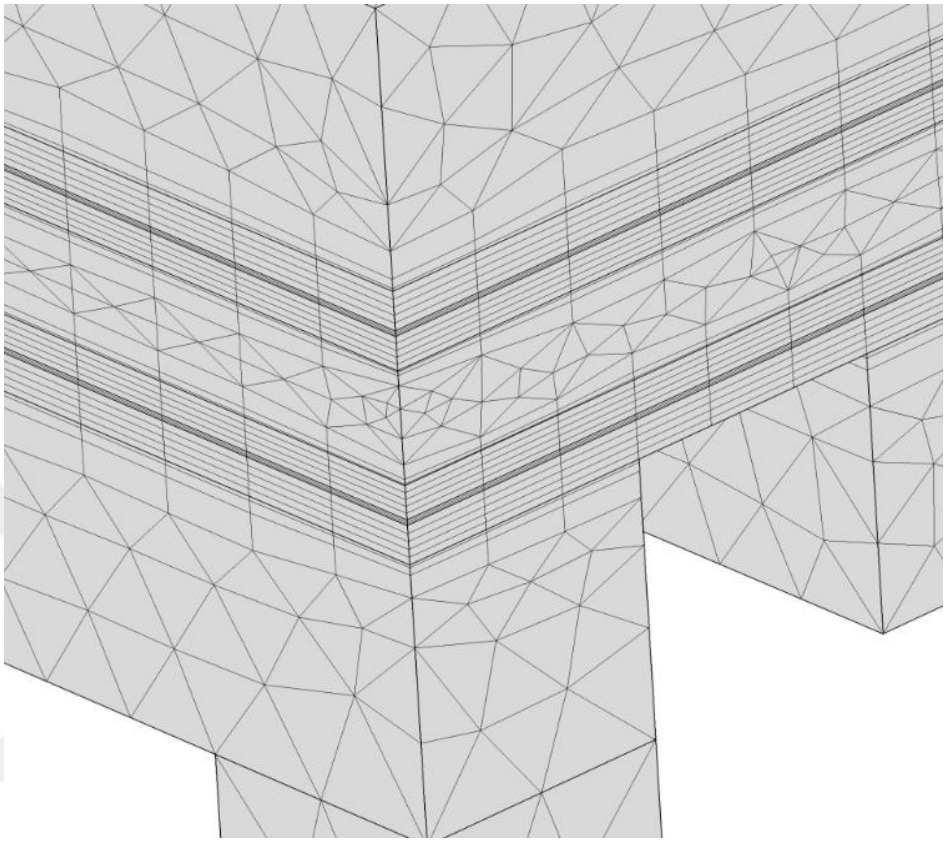

Figure 3.8 Mesh Generations of Each Layer

3.5.4 Post Processing

The results after the analysis will be interpreted using the modules found under the Comsol results section. When these interpretations are made, mostly the plot groups and plots, and derived values and tables modules will be used. A plot group is a collection of plots to display simultaneously in the Graphics window. You can enable or disable plots in a plot group to determine the most applicable final image for your model or project. The physics interfaces create suitable default plots grouped in descriptive plot groups. Use a combination of data sets and plot groups to create cross-section plots. Derived values define the evaluation of integrals, maximum and minimum values, values of variables in points, and values of global

variables. The evaluation results are stored in tables and displayed in the Table window.

CHAPTER FOUR
RESULTS AND DISSCUSSION

4.1 Validation of the Model

In this section, polarization and power curves were obtained by experimentally examining the MED3036 coded membrane electrode assembly (MEA) with 25 cm^2 (5 cm x 5 cm) active area of IRD which is a company that product the MEA used in experimental studies. In this context, flow channels were cleaned with a brush to remove undesired particles before placing them in the cell to test the membrane electrode component. Parallel serpentine flow channels can be seen in Figure 4.1. After canal cleaning, the active area of the membrane electrode component was placed in the cell corresponding to the 25 cm^2 active area of the cell, and the sealing elements were fitted. To prevent leaks and obtain co-pressure distributions in the cell, the cells in the cell were closed in the order shown in Figure 4.2. The cell temperature was set at 80 ^oC from the computer interface and the data input was made by setting the methanol tank outlet temperature at 75 ^oC so that the cell temperature could be stabilized at 80 ^oC. In order to perform the activation process of the membrane electrode component, oxygen was sent by the anode for 4 hours by pure water and cathode by 2 $L.min^{-1}$ flow rate and by 10 $ml.min^{-1}$ flow rate. Through the activation process, the membrane was humidified and reached the working temperature. A methanol-pure water mixture prepared in 1 M concentration was added to the methanol tank of the test station as shown in Figure 4.3 where the experimental work was carried out. During the experiment, the methanol-pure water mixture was sent to the anode side of the cell by 1.94 $ml.min^{-1}$, while the oxygen gas was sent to the cathode side of the cell by 0.2 L. min^{-1}. After the cell reaches a stable open-circuit voltage (OCV), the current and power values are recorded by stepping down to 0.2 V with a step of 0.05 V.

Figure 4.5 shows the model of the fuel cell in the experimental setup. During this modelling, the program was defined to be the same as the fuel cell measurements and the appropriate design and operating parameters were taken and analysed.

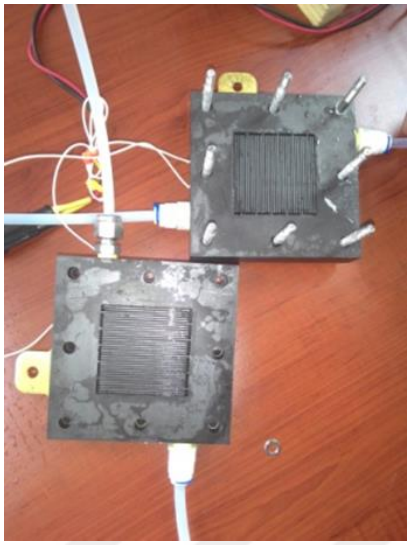

Figure 4.1 Flow Field of Test Station Fuel Cell

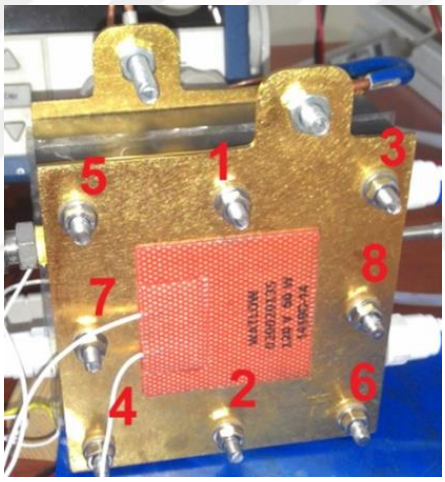

Figure 4.2 The Sequence of Tightening Bolts

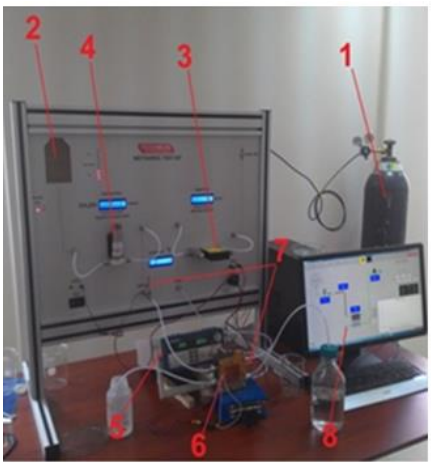

1	Oxygen Tube
2	Methanol Tank
3	Gas Flow Controller
4	Pump
5	Load Bank
6	Fuel Cell
7	Thermocouple
8	Computer

Figure 4.3 Direct Methanol Fuel Cell Test Station and Auxiliary Components

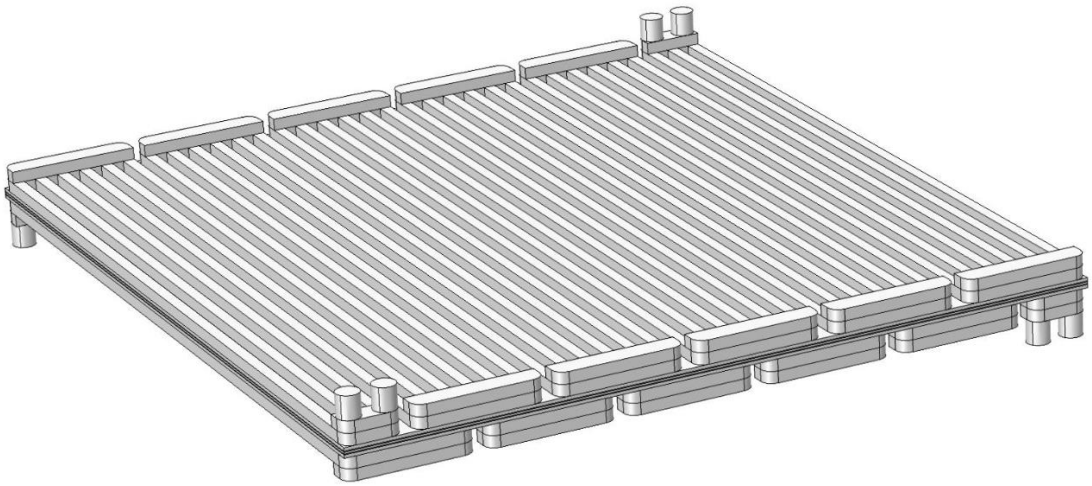

Figure 4.5 3D Geometry of DMFC at Dokuz Eylül University Test Station

The layers and channel measurements of the DEU fuel tank are given in Table 4.1.

Table 4.1 DEU fuel cell geometric measurements

Active area (cm^2)	25
Channel width (mm)	0.75
Channel depth (mm)	0.75
Backing Layer thickness (mm)	0.21
Catalyst Layer thickness (mm)	0.05
Membrane thickness(mm)	0.12

Experimental results were compared with the data obtained by the experiments as described in validation of the model section. The operating conditions and input variables are modelled by selecting the same as the experimental work. Then the model is operated parametrically for 0.3-0.7 V values. As can be seen in Figure 4.4, the difference in the values of the high current density can be attributed to the simplified electrochemical equations of the equations used for the volumetric current density. Moreover, negligible effects of water and carbon dioxide bubbles due to the neglect of the two phase effect on the cell voltage have been overlooked. However, the difference between the experimental results and the model results (%95 conformity) for the operating voltage range is acceptable.

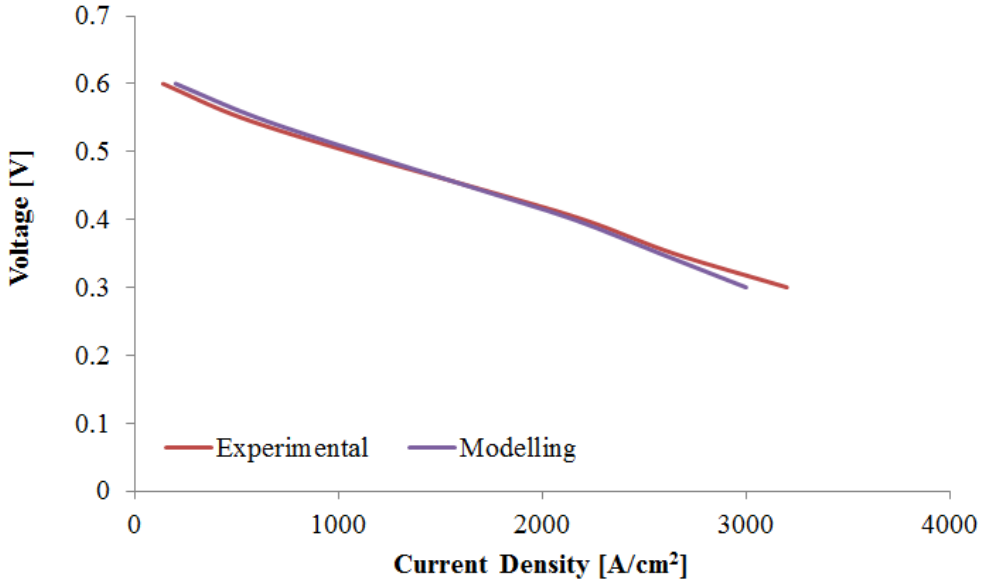

Figure 4.5 DMFC polarization curve; comparison of experimental data with numerical data

4.2 Pressure and Velocity Distributions

In each of the four configurations, shown in Figure 4.6, it can be seen that the single serpentine design had the highest pressure drop of ~350 Pa, whereas the grid flow field had the lowest pressure drop ~5 Pa. The pressure difference for the remaining two configurations are: ~50 Pa for the parallel serpentine design and ~35 Pa for the triple serpentine design. The large difference in the pressure drops for each case is due to the difference in the number of bends and channels. In the case of the single serpentine flow field, the supplied air only travels through one channel and makes 16 turns. Forcing the air to move at a high velocity, for the same volume flow rate, through one channel (refer to Figure 4.7 for the velocity distributions within each cathode channel configuration). This turning leads the air to have a high degree of momentum, requiring a high pressure difference to transport the air around the bends. Within the grid configuration, the air has a very large open area, allowing the air to move at a much smaller velocity and thus momentum; requiring a lower pressure difference to move the air from the inlet to outlet. Between the parallel and triple serpentine designs, the parallel serpentine flow field had the higher pressure drop due to the fact that the reactant's flow was forced through a single narrow

channel at each of the bends. This in turn required a higher pressure difference to move the fluid at the increased velocity at the bends.

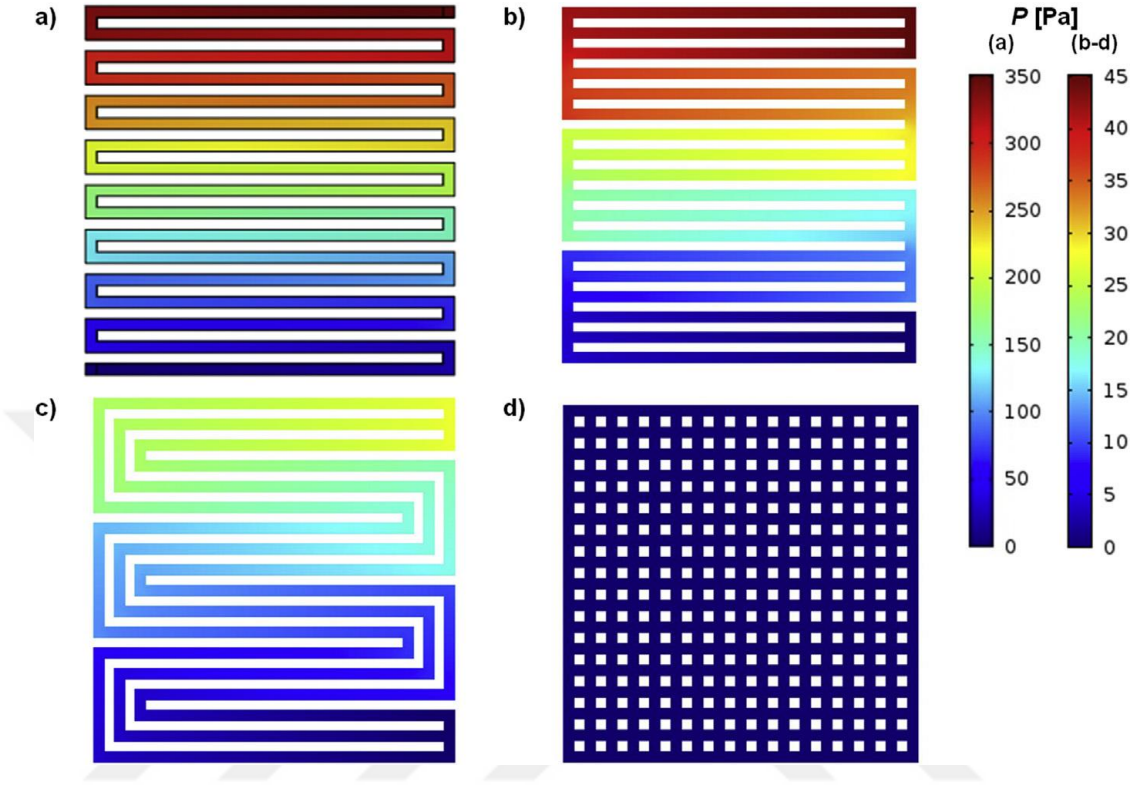

Figure 4.6 Pressure distributions in the center width of each flow field: a) serpentine, b) parallel serpentine, c) triple serpentine, and d) grid

It should also be noted that the grid flow field was susceptible to stagnate (low velocity) patches, as can be seen in Figure 4.7d's top-left side and bottom-right side corners. This is primarily due to the positions of the inlet and outlet manifolds. Since the pins provide little resistance to the overall fluid motion, the fluid can therefore travel from the inlet to the outlet very easily. Resulting in a nearly linear flow direction (from inlet to outlet), giving rise to the observed low velocity patches. As will be discussed in section “Oxygen concentration distribution”, these locations cause a diffusion-dominated zone, which are susceptible to mass transport limited conditions are low current densities, relative to the remaining areas of the fuel cell. Indicating that the grid flow field's inlet and outlet would require special consideration to ensure such conditions do not occur. Furthermore, the remaining configurations do not have the aforementioned issue, due to the tortuous channel paths. However, the under-rib zones would be susceptible to mass transport limited

conditions, under high current density conditions; assuming two-phase effects (e.g.: water flooding) is not an issue. This would be due to their dependence on cross-diffusion and under-rib convection to maintain a relatively uniform concentration distribution.

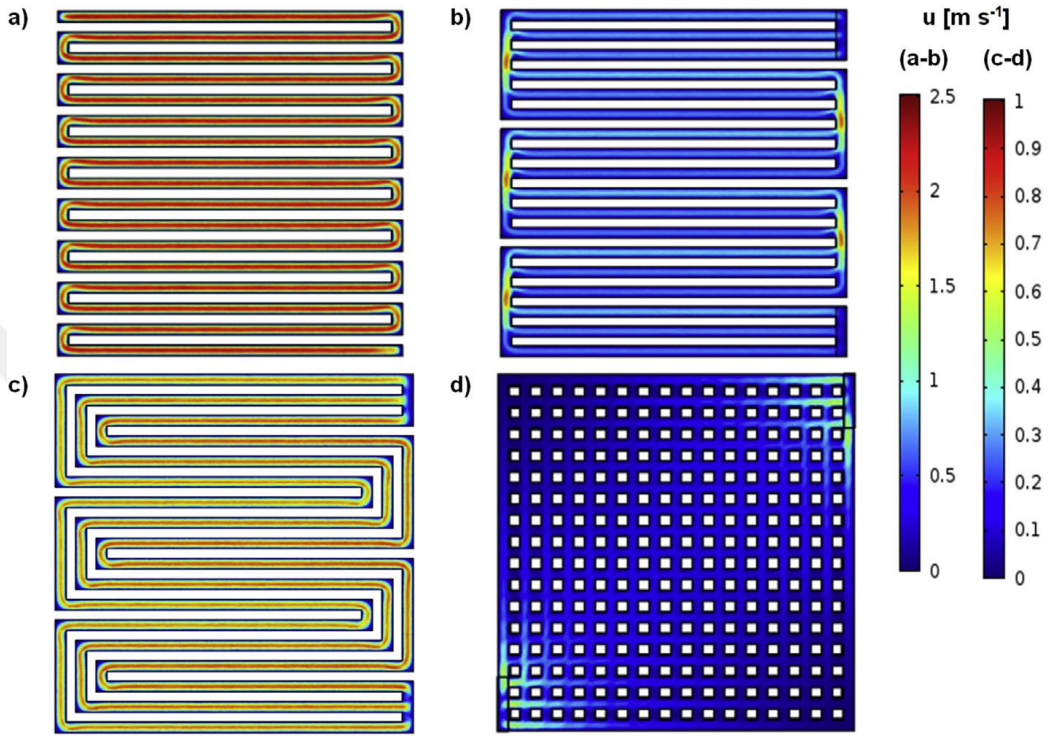

Figure 4.7 Velocity distribution in the center width of each flow fields at a current density of 3000 Am^{-2}: a) serpentine, b) parallel serpentine, c) triple serpentine, and d) grid

4.3 Methanol Concentration Distribution

As can be seen in Figure 4.8, the methanol concentration field follows a decreasing trend from anode to cathode, which is attributed to the consumption of methanol within the ACL. A low methanol concentration of was found under the AFC's ribs, since the rib acts as a wall. However, within the anode's flow field, under-rib convection was observed as there was significant pressure difference between channel passes, driving methanol from one channel to the next through the ABL. This was accentuated at higher current densities, as more methanol was driven through the ABL towards the ACL to be consumed, but also towards the adjacent channel. This can be seen in Figure 4.8.

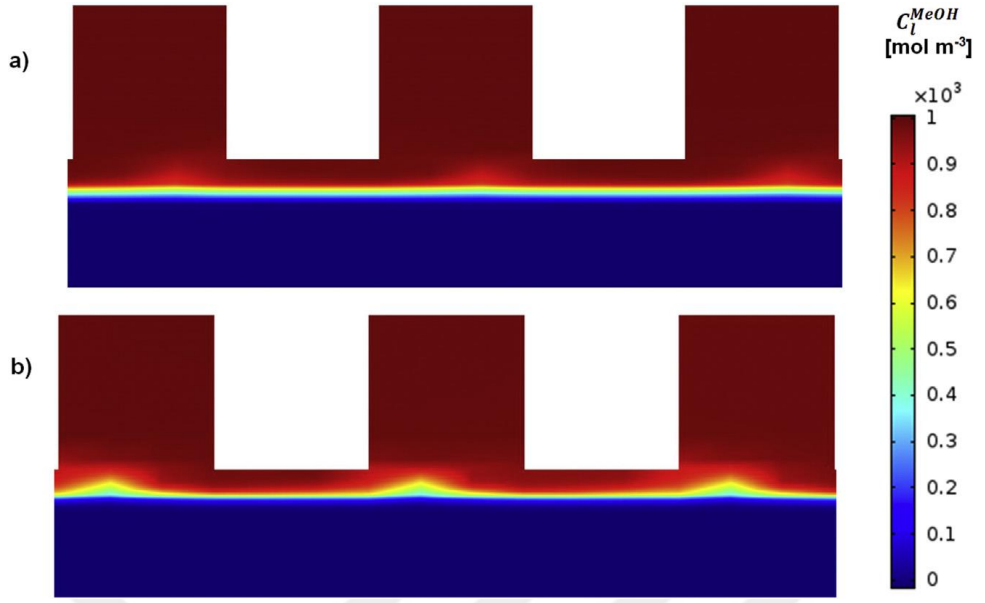

Figure 4.8 Methanol concentration of fuel cell at a current density of: a) 500 A m^{-2}, and b) 2500 A m^{-2}

Unreacted methanol is transported through the AM towards the cathode through diffusive and electro-osmotic driving forces. However, due to the strong convective flux within the FEC, the majority of methanol is removed from this channel, protecting the cathode from methanol crossover. In Figure 4.9, it can be seen that the local methanol concentration at the middle of the FEC is very low, <8 mol m^{-3}, indicating a very low crossover current density, as displayed in Figure 4.10. Comparing to the previous studies, the predicted crossover current densities are approximately 4 times higher than those of the studies' 1D model (Ouellette, Colpan, Matida, Cruickshank, 2015). This could be attributed to the fact that the 1D model assumes that the results are averaged across the CM-CCL interface, whereas the 3D model accounts for the actual flux distribution across the CM-CCL interface. However, the two models do provide comparable predictions and the magnitude of the flux suggests that the crossover current density could be considered to be negligible. An advantage of this low methanol permeation rate, is that the Faradaic efficiency, given by Equation (4.1), is greater than 95%, even at near-OCV conditions (i_{cell} = 10 A m^{-2}). This is a significant improvement, compared to the DMFC, which have only achieved comparable Faradaic efficiencies at very high current densities. Although this calculation does not account for the methanol removed at the AFC and FEC outlets, it should be noted that on a system-level, the

removed methanol would be separated and reused at the anode inlet. Therefore, making those contributions equal to zero in Equation (4.1).

$$\varepsilon_{faradaic} = \frac{i_{cell}}{i_{cell}+i_{xover}} \tag{4.1}$$

However, at much lower FEC flow rates (e.g.: 1 mL min^{-1}), the crossover current density increased proportionally (tenfold) due to the decreased crossflow within the FEC.. For example, a Faradaic efficiency of 29% was obtained for the single, parallel and triple serpentine configurations, whereas the Faradaic efficiency was 28% for the grid flow field; all at near-OCV conditions (i_{cell} = 10 A m^{-2}). These differences were found to be associated with the differences in through-plane convection between the examined cathode flow field configurations.

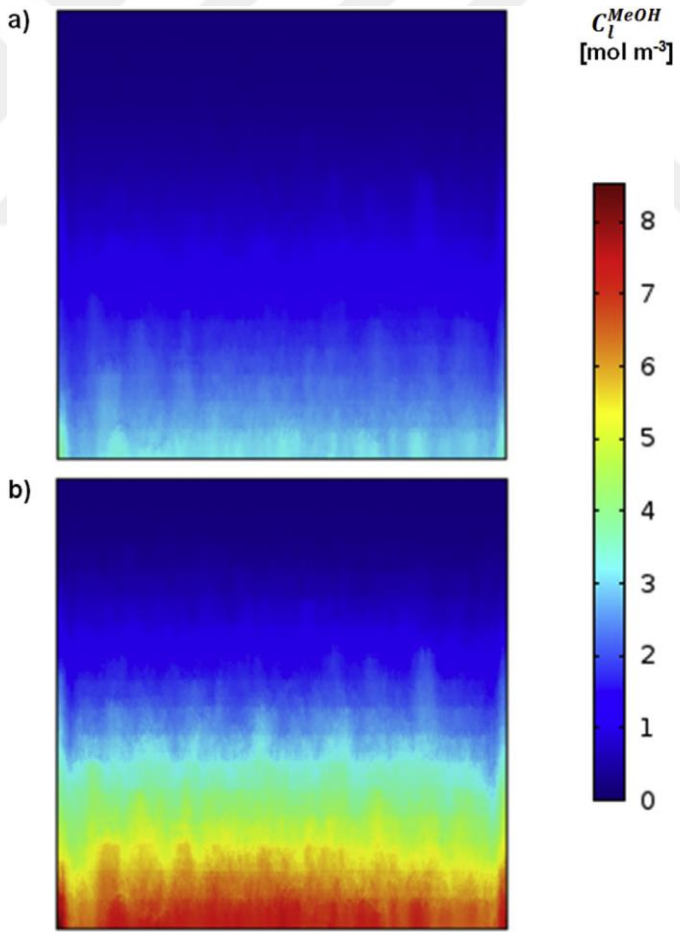

Figure 4.9 Methanol concentration distributions in the mid plane of the FEC at a current density of: a) 500 A m^{-2}, and b) 2500 A m^{-2}

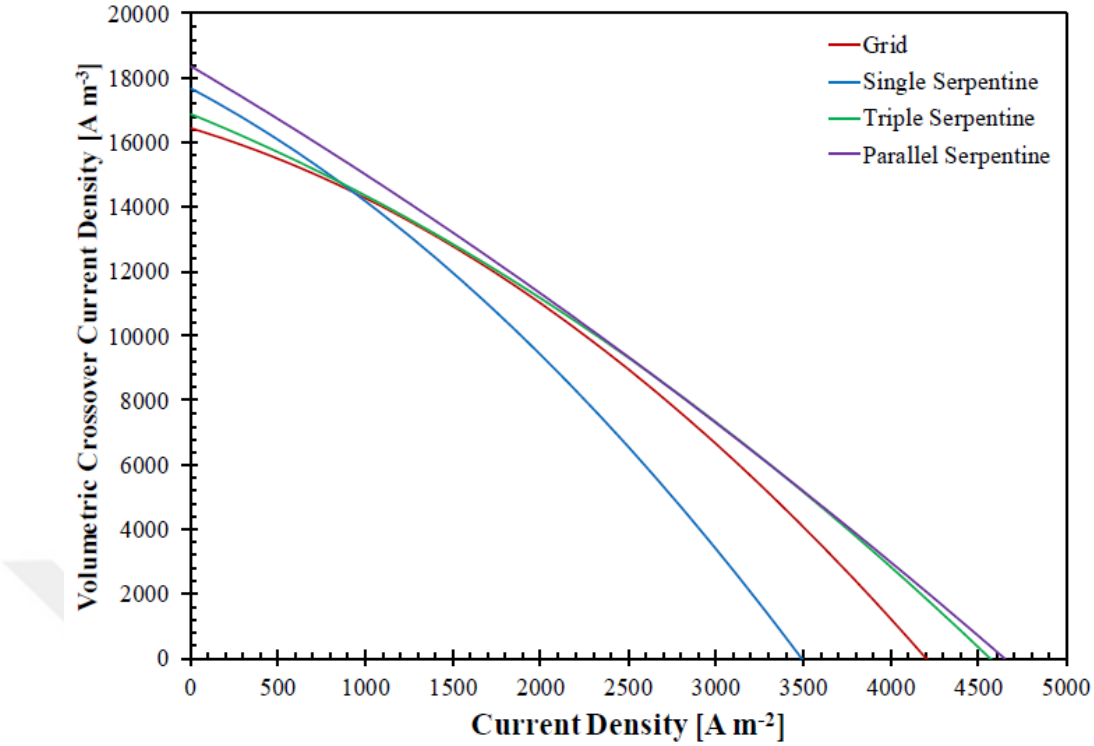

Figure 4.10 Volumetric crossover current density distributions for each cathode flow field configuration

4.4 Oxygen Concentration Distribution

As was discussed in Section "Pressure and velocity distributions", the single serpentine flow field provided the highest velocity within the CAC. This in turn caused the oxygen concentration to be the most uniform relative to the remaining flow field configurations, as shown in Figure 4.11. As the number of channels within the flow field increased, the mean velocity within the channels decreased. As such, this caused the grid flow field, which had the lowest mean velocity of the examined CACs, to have the least uniform concentration distribution of the tested configurations, where low concentration zones, or "dead zones" were observed near the top-left and bottom-right of the flow field. These dead zones were also attributed to the fact that the ribs within the grid flow field allowed the supplied oxygen to move diagonally from inlet to outlet directly, with little resistance; causing near-stagnant zones, as discussed in Section "Pressure and velocity distributions". As such, little of the oxygen reached the dead zones, which caused a locally diffusive-dominated regime, which is comparatively a much slower transport process. In each

of the serpentine-based flow fields, this was less of an issue as oxygen was forced to follow the channel's path. However, the lowest concentration was achieved near at the cathode's outlet. For the serpentine-based flow fields, the oxygen concentration underneath the ribs could also become a challenge. Although this is less of an issue on the cathode, when compared to the anode, due to oxygen's higher diffusivity than that of methanol's.

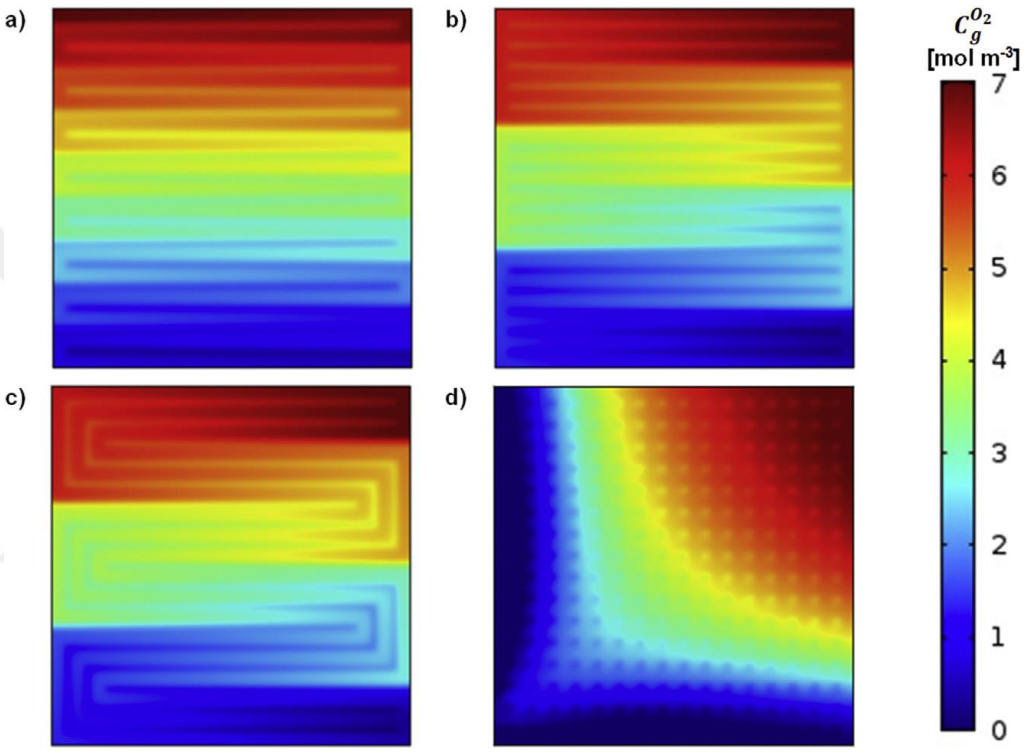

Figure 4.11 Oxygen concentration in the middle of CCL for each flow field at a current density of 2500 A m^{-2}: a) serpentine, b) parallel serpentine, c) triple serpentine, d) grid

4.5 Cathode and Anode Activation Polarization

The cathode activation polarization curve is shown in Figure 4.12 for different flow field configurations. At low current densities (<2000Am^{-2}), the oxygen consumption is close to each other for four different flow channel designs, and the cathode activation polarization shows a close proximity to each other. At high current density values (>2000Am^{-2}), the amount of oxygen that reaches the catalyst layer varies depending on the difference in the flow channel design. This causes a difference in the oxygen reduction reactions. From these reactions, the highest

cathode activation polarization values are given by grid flow channel design and the lowest cathode activation polarization values are given by serpentine flow channel design. The high activation polarization values, depending on equation 3.7, affect battery performance negatively.

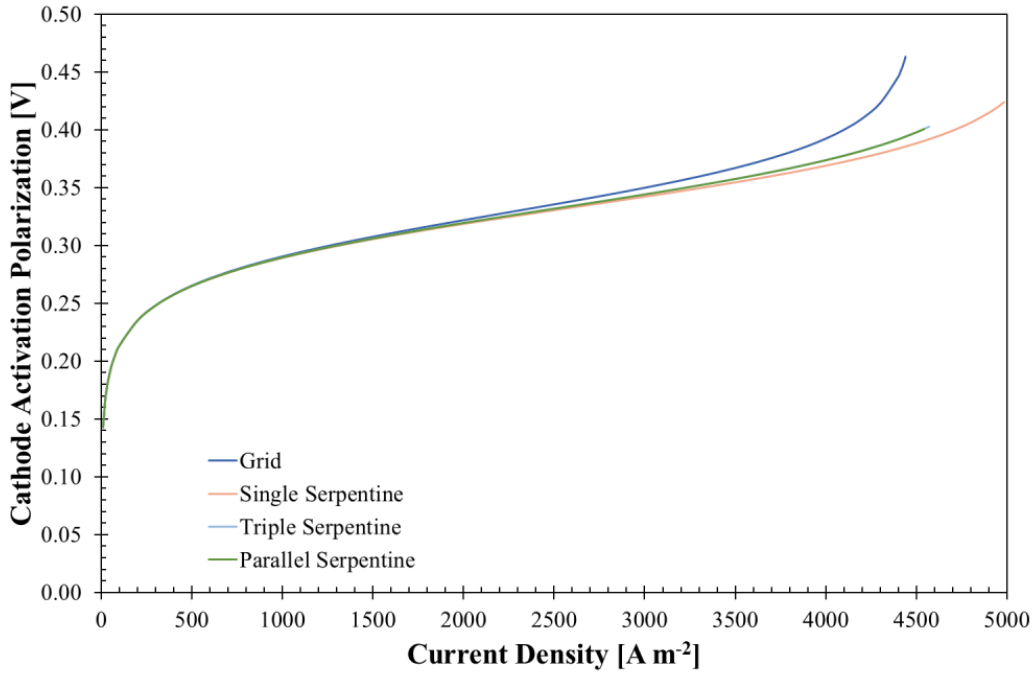

Figure 4.12 Cathode activation polarization curve for each flow field configuration

4.6 Cathode Concentration Polarization

The concentration polarization, the thermodynamic voltage in the Nernst equation and the change in the Butler-Volmer equation occur with a decrease in the reactant surface concentration, which reduces the current density. As well as reduced reactant transfer due to the amount of reactant present on the surface of the catalyst layer. This decrease depends on the amount of oxygen present on the surface depending on the flow field channel design. As can be seen in Figure 4.13, these effects are most visible in grid flow channel design. Single serpentine flow channel configuration gives the lower cathode activation polarization. The reactant transfer from the high pressure differential coming from the column in the serpentine flow channel design is faster to the catalyst bed and hence the reaction rate is higher. This prevents the

accumulation of reactants that can occur on the surface and provides less display of concentration polarization.

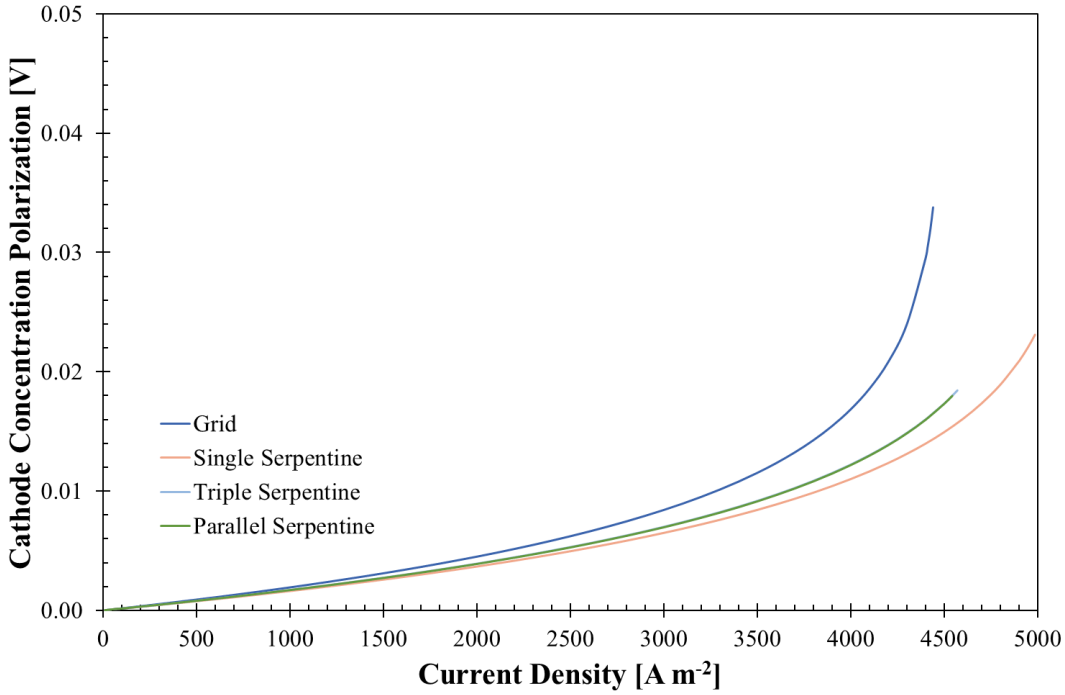

Figure 4.13 Cathode concentration polarization curve for each flow field configuration

4.7 Polarization Curve

The polarization curves for each flow field configuration are shown in Fig. 4.14. As discussed in Sections "Methanol Concentration Distribution" and "Oxygen Concentration Distribution", the velocity distribution within the CAC had the greatest impact in the oxygen's concentration distribution. At low current densities (<2000 A m^{-2}), all flow fields performed similarly, primarily due to the low consumption rate within the CCL (associated with low current densities), and also due to the fact that the FEC nearly eliminated all methanol crossover ($j_{xover,max}$=18,400 A m^{-3}). At higher current densities (>2000Am^{-2}), the grid flow field yielded the lowest performance due to a more significant cathode concentration polarization, due to the described dead zones near the top-left and bottom right of the cathode flow field. The grid configuration's limiting current density was found to be ~4440 A m^{-2}. On the other hand, the single serpentine flow field, which had the

greatest channel velocity and best oxygen coverage within the cathode, was able to obtain much higher limiting current densities (~5000 A m^{-2}).The remaining serpentine designs obtained comparable results as their velocity and oxygen concentration distributions within the cathode were comparable. For comparison, the cathode's concentration polarizations at limiting current were found to be: 23.1 mV for the single serpentine, 18.4 mV and 18.0mV for the parallel and triple serpentine flow fields respectively, and 34.5mV for the grid flow field.

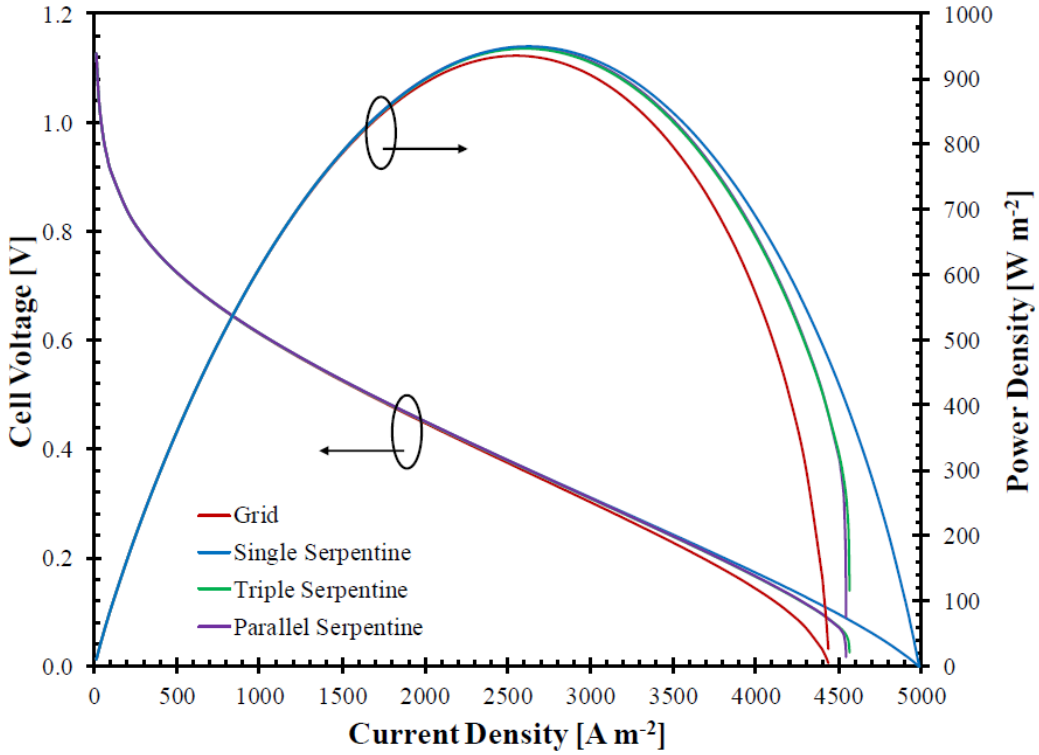

Figure 4.14 Polarization curve for each cathode flow field configuration

4.8 Effect of Flowing Electrolyte Flow Rate

The electrolyte flow rate is one of the most important input parameters affecting the performance of an FE-DMFC. Depending on this flow rate, the amount of methanol reaching the CCL, the crossover current density of the cell, the polarization of the cathodic activation increases, which causes a decrease in cell voltage and power density. The effect of electrolyte flow rate on cell voltage is shown in Figure 4.15, respectively. When we compare the performance of the low flow rate with the

performance of the high flow rate, 0.1 ml min^{-1} and 10 ml min^{-1} provide better performance with the flowing electrolyte channel with a higher flow rate. For example at current density is 4000 A/m^{-2}; flow rate 10 ml/min^{-1} voltage is 0.21 V, flow rate 1 ml/min^{-1} voltage is 0.19 V, flow rate 0.1 ml/min^{-1} voltage is 0.16 V. In operation with a high flowing electrolyte channel velocity, the flowing electrolyte will carry more methanol out of the cell and prevent crossover polarization on the cathode side. Also, inhibiting the passage of methanol on the cathode side causes the active area to not reduce and cell performance is positively affected.

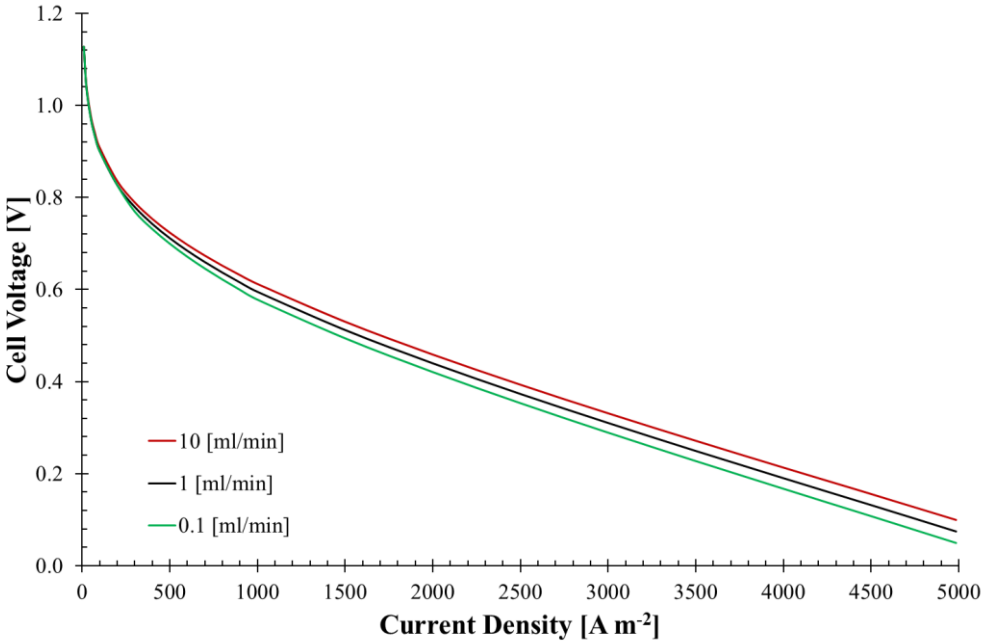

Figure 4.15 Effect of flowing electrolyte flow rate

4.9 Effect of Flowing Electrolyte Thickness

Determination of flowing electrolyte channel thickness is another important design parameter for FE-DMFCs. For an FE-DMFC operating in a sufficient amount of electrolyte flow, the change in electrolyte flow mainly affects the ohmic polarization of the cell. Figure 4.16 shows the ohmic polarization of an FE DMFC at 1 mm, 0.61 mm and 0.1 mm electrolyte channel thicknesses. For the comparison shown in Figure 4.17, the change in the total ohmic polarization of an FE-DMFC with the thickness of the flowing electrolyte channel is due only to changes in these

flowing electrolyte channel thicknesses. The effects of fluid electrolyte channel thickness, cell voltage and power density on FE-DMFC are shown in Figure 4.16, respectively. For thicker electrolyte channels, ohmic polarization is higher and performance is lower for these conditions. In addition, for thicker channels, as the total thickness of a single cell increases, the volumetric power density of the system is reduced.

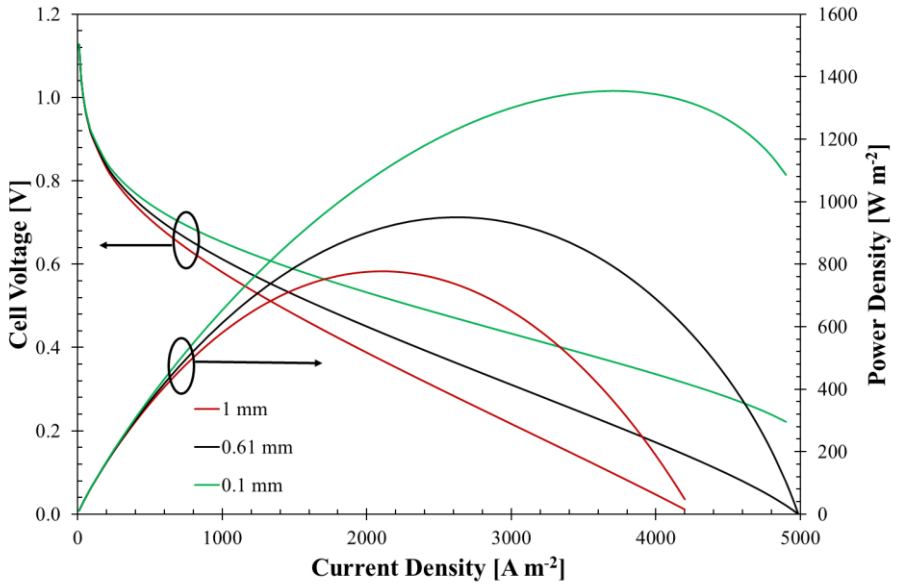

Figure 4.16 Effect of flowing electrolyte thickness

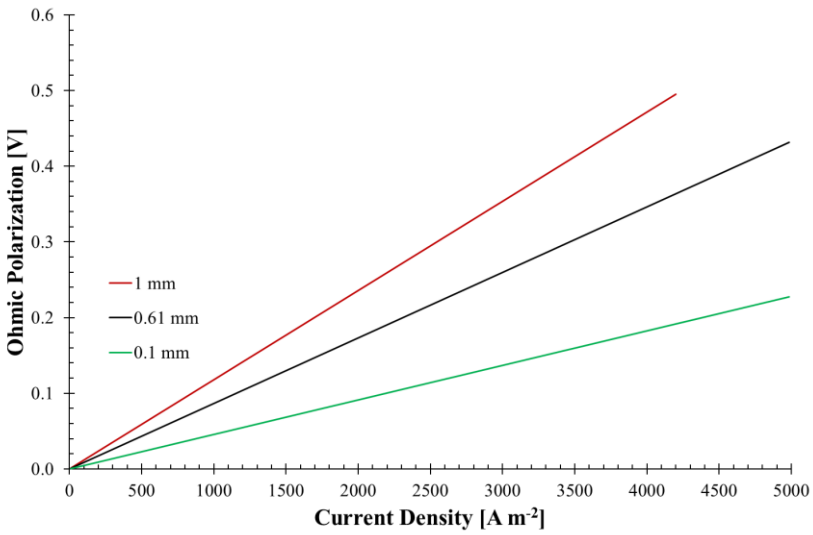

Figure 4.17 Effect of the thickness of flowing electrolyte channel on the ohmic polarization

4.10 Effect of Fuel Cell Temperature

Increasing the operating temperature of the fuel cell accelerates the reaction kinetics, while also increasing the permeability of Nafion® to methanol. Figure 4.18 shows the performance of the fuel cell at operating temperatures of 70, 80 and 90 ° C, where 1M methanol and 0.6 mm FE channels are used. The fuel cell operating at 80 ° C produces the highest power density, which is approximately 901 W / m2. These behaviours indicate that the methanol crossover does not affect the performance of the cell because of the high temperature. The polarization curve shows that the decrease in activation is reduced with increasing temperature. In this study, modelling at higher temperatures was not considered suitable due to the electrodes and Nafion®'s temperature limitations.

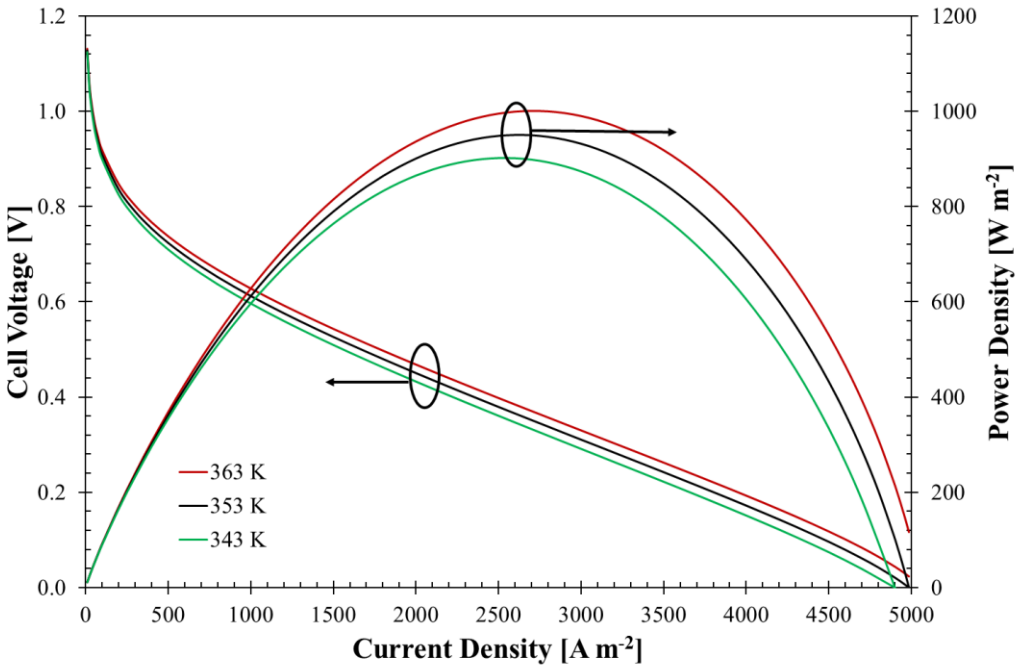

Figure 4.18 Effect of fuel cell temperature

4.11 Effect of Methanol Concentration at Feed Stream

Figure 4.19 shows the polarization curves at different methanol flow rates. The temperature of the cell is 80 °C and the methanol concentration is 1 M. A significant increase in fuel cell performance was observed due to increased flow rate. The

highest power value was obtained at a flow rate of 15 ml/min, which is approximately 1125 W / m2. At low flow rate values, depending on the mass transfer resistance, the methanol concentration is very low in the catalyst layer and causes a lower current density, especially downstream. Since the flow rate is sufficiently high when the flow rate is higher than 15 ml / min, any increase in flow rate does not have a significant effect on the methanol concentration in the channel and the catalyst layer, so that the flow rate does not have a significant effect on the cell performance.

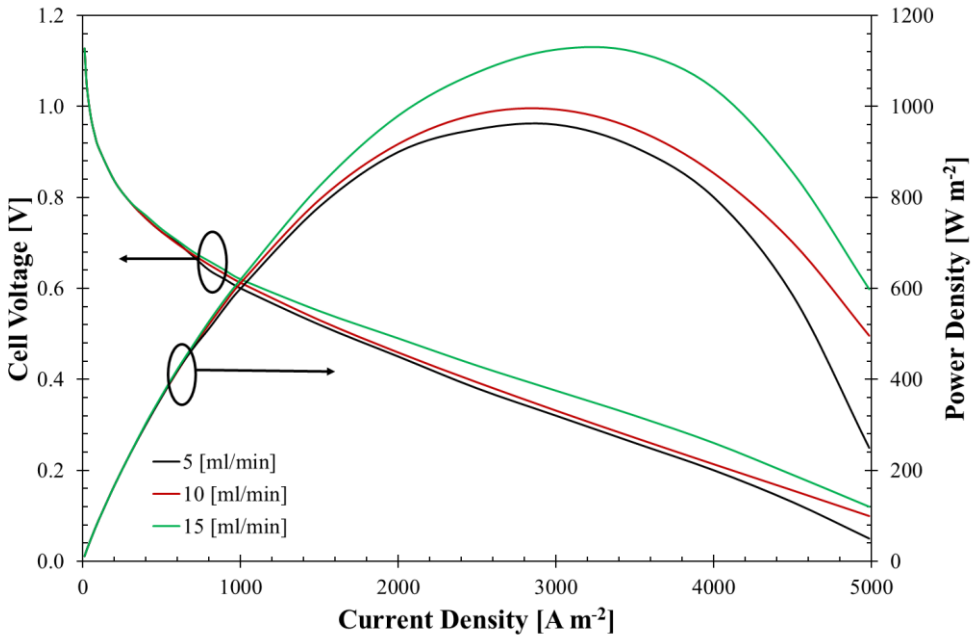

Figure 4.19 Effect of methanol flow rate

CHAPTER FIVE
CONCLUSIONS

A 3D, single phase FE-DMFC with four different cathode channel configurations (serpentine, parallel serpentine, triple serpentine and grid) is modelled. The effect of current density on the methanol concentration at the middle of the FEC and the observed causes are investigated. Of the examined flow fields, the single serpentine flow field provided the best performance as this provided the greatest oxygen coverage on the CCL. Comparatively, the grid type flow field provided the lowest performance, as the hydrodynamics within the channel caused locally diffusive-driven transport, which in turn lead to dead zones and a mass transport limitation regime. The following conclusions were obtained in summary;

- The best performance was observed in the design of a single serpentine flow channel.
- The methanol constancy difference at the inlet and outlet was observed at the maximum in the single serpentine flow channel since the channel length in the single coil was greater than in other designs.
- However, since increasing the speed of fuel entering the fuel duct can create sealing problems in practice, the applications require that the mechanical tests and analyses should be at a determined speed,
- An increase in temperature of cell affects cell performance positively,
- It has been observed that the increase in the flow rate of the flowing electrolyte affects the cell performance in the positively and the increase in the thickness in the negatively. These two parameters need to be optimized by verifying their optimal working range.

REFERENCES

Arico, A., S., Creti, P., Baglio V., Modica, E., Antonucci V. (2000). Electrocatalysist of Direct Methanol Fuel Cells. *Journal of Power Sources, 91,* 202.

Baglio, V., Blasi, A. D., Arico, A. S., Antonucci, V., Antonucci, P., L. (2004). Influence of TiO_2 nanometric filler on the behaviour of a composite membrane for applications in direct methanol fuel cells. *Journal of New Mater Electrochemistry, 280,* 275-280.

Barbir, F. (2013). *Pem fuel cells theory and practice* (2th ed.). California: Elsevier.

Colpan, C., O., Cruickshank, C., A., Matida, E., Hamdullahpur, F. (2011). 1D modelling of a flowing electrolyte-direct methanol fuel cell. *Journal of Power Sources, 196,* 3572-3582.

Colpan, C., O., Fung, A., Hamdullahpur, F. (2012). 2D modelling of a flowing-electrolyte direct methanol fuel cell. *Journal of Power Sources, 209,* 301-311.

Duivesteyn, E., Cruickshank, C., A., Matida, E. (2013). Modelling of a porous flowing electrolyte layer in a flowing electrolyte direct-methanol fuel cell. *International Journal of Hydrogen Energy, 38,* 13434-13442.

Jung, G., B., Su, A., Tu, C., H., Lin, Y., T., Weng, F., B., Chan, S., H. (2007) Effects of cathode flow fields on direct methanol fuel cell-simulation study. *Journal of Power Sources, 171,* 212-217.

Jung, G., B., Tu, C., H., Chi, P., H., Su, A., Weng, F., B., Lin, Y., T., et al. (2009). Investigations of flow field designs in direct methanol fuel cell. *J Solid State Electrochem, 13,* 1455-1465.

Kjeang, E., Goldak, J., Golriz, M., R., Gu, J., James, D., Kordesch, K. (2006). A parametric study of methanol crossover in a flowing electrolyte-direct methanol fuel cell. *Journal of Power Sources, 153*, 89-99.

Kjeang, E., Goldak, J., Golriz, M., R., Gu, J., James, D., Kordesch, K. (2005) Modeling methanol crossover by diffusion and electro-osmosis in a flowing electrolyte direct methanol fuel cell. *Fuel Cells, 5*, 486-498.

Kordesch, K., Hacker, V., Bachhiesl, U. (2001) Direct methanol air fuel cells with membranes plus circulating electrolyte. *Journal of Power Sources, 96*, 200-203.

Larminie, D., & Dicks, A. (2003). *Fuel cell system explained* (2th ed.). West Sussex: Wiley

Matthew, M. (2008). *Fuel cell engines* (1st ed.). New Jersey: Wiley.

Ouellette, D., Colpan, C., O., Matida, E., Cruickshank, C., A., Hamdullahpur F. (2015). A comprehensive 1D model of a flowing electrolyte-direct methanol fuel cell with experimental validation. *International of Journal Energy Resources, 39,* 33-45.

Ouellette, D., Colpan, C., O., Matida, E., Cruickshank, C., A., Hamdullahpur F. (2015). A comprehensive 1D model of a flowing electrolyte-direct methanol fuel cell with experimental validation. *International Journal of Energy Resources, 39,* 33-45.

Sabet-Sharghi, N., Cruickshank, C., A., Matida, E., Hamdullahpur, F. (2013). Performance measurements of a single cell flowing electrolyte-direct methanol fuel cell (FE-DMFC). *Journal of Power Sources, 230,* 194-200.

USFCC Single Cell Test Protocol. (2006) Retrieved July 9, 2013, from http://www.members.fchea.org/core/import/PDFs/Technical%20Resources/Mat

Comp%20Single%20Cell%20Test%20Protocol%2005-014RevB.2%20071306.pdf.

Vera, M. (2007). A single-phase model for liquid-feed DMFCs with non-Tafel kinetics. *Journal of Power Sources, 171*, 763-777.

Yang, H., Zhao, T., S. (2005). Effect of anode flow field design on the performance of liquid feed direct methanol fuel cells. *Electrochimica Acta, 50*, 3243-3252.

Zeng J., Yang J. (2007) Ruthenium-free, carbon-supported cobalt and tungsten containing binary & ternary Pt catalysts for the anodes of direct methanol fuel cells. *International Journal of Hydrogen Energy, 32*, 4389-43996.

APPENDIX

Nomenclature

Abbreviations

ABL	Anode backing layer
ACL	Anode catalyst layer
AFC	Anode fuel channel
AM	Anode membrane
CAC	Cathode air channel
CBL	Cathode backing layer
CCL	Cathode catalyst layer
CM	Cathode membrane
DMFC	Direct methanol fuel cell
FEC	Flowing electrolyte channel
FE-DMFC	Flowing electrolyte-direct methanol fuel cell
OCM	Open circuit voltage
MOR	Methanol oxidation reaction

Variables

ai_o	Reference exchange current density, A m^{-3}
D	Diffusion coefficient, m^2 s^{-1}
F	Faraday constant C mol^{-1}
i	Current density, A m^{-2}
j	Volumetric current density, A m^{-3}
j_{xover}	Crossover current density, A m^{-3}
K_c	Reaction constant for methanol oxidation, mol m^{-3}
M	Molecular weight, kg mol^{-1}
n_d	Coefficient of electro-osmotic drag, unitless
P	Pressure, Pa

R	Universal gas constant, J mol^{-1} K^{-1}
S_{gen}^{k}	Molar consumption/generation flux of species k, mol m^{-3} s^{-1}
T	Temperature, K
$\boldsymbol{u}$	Velocity, m s^{-1}
V	Cell voltage, V

Greeks Letters

ν	Kinematic viscosity, m^2 s^{-1}
μ	Dynamic viscosity of fluid, kg m^{-1} s^{-1}
α	Transfer coefficient, unitless
ε	Porosity, unitless
η	Overpotential, V
κ	Permeability, m^2
ρ	Density, kg m^{-3}

Subscript/Superscript

a	Anode
c	Cathode
channel	Channel
H_2O	Water
in	Inlet
k	Species
l	Liquid phase
mem	Membrane
MeOH	Methanol
O_2	Oxygen
out	Outlet
ref	Reference value
Ref	Reference

xover	Crossover